

Phase diagram of the magnetized planar Gross-Neveu model beyond the large- N approximation

Jean-Loïc Kneur,^{1,2,*} Marcus Benghi Pinto,^{3,†} and Rudnei O. Ramos^{4,‡}

¹*CNRS, Laboratoire Charles Coulomb UMR 5221, F-34095, Montpellier, France*

²*Université Montpellier 2, Laboratoire Charles Coulomb UMR 5221, F-34095, Montpellier, France*

³*Departamento de Física, Universidade Federal de Santa Catarina, 88040-900 Florianópolis, Santa Catarina, Brazil*

⁴*Departamento de Física Teórica, Universidade do Estado do Rio de Janeiro, 20550-013 Rio de Janeiro, RJ, Brazil*

The phase diagram and thermodynamic properties of the (2+1)-dimensional Gross-Neveu model are studied in the presence of a constant magnetic field. The optimized perturbation theory (OPT) is used to obtain results going beyond the large- N approximation. The free energy and the complete phase diagram of the model, in terms of temperature, chemical potential and magnetic field are obtained and studied in details. We find that some of the main qualitative changes induced by the OPT finite N corrections concern the region of intermediate to high chemical potentials where this approximation adds a term proportional to $\lambda\langle\psi^+\psi\rangle^2/N$ to the free energy. Then, depending on the sign of λ (relative to the critical coupling), and magnitude of the magnetic field, we observe a weakening (when $\lambda < 0$) or enhancement (when $\lambda > 0$) of the chiral broken region in the magnetized fermionic system. By comparing the results from the OPT and the large- N approximation, we conclude that finite N effects favor the phenomenon of inverse magnetic catalysis when the coupling constant is negative. We show that with the OPT the value of the coexistence chemical potential at vanishing temperature tends to decrease for large values of the magnetic field. This is opposite to what is seen in the large- N approximation, where for large magnetic fields the coexistence chemical potential starts again to increase. Likewise, at finite temperature, the value of the chemical potential at the tricritical point also decreases with the magnetic field in the OPT case. Consequently, the shape of the phase diagrams predicted by the OPT and by the large- N approximation look very different in the presence of high magnetic fields. Finally, for small values of magnetic field and temperature, we identify the presence of possible intermediate nonchiral phase transitions when varying the chemical potential. We show that these phenomena are not an artifact of the large- N approximation and that they also occur within the OPT framework. These intermediate transitions are interpreted to be a consequence of the de Haas-van Alphen oscillations. We also explain why this type of phenomenon can happen in general for negative couplings but not for positive couplings.

PACS numbers: 11.10.Wx, 12.38.Cy, 11.15.Tk, 11.30.Rd

I. INTRODUCTION

Four-fermion theories [1] find applications in several areas of physics, from condensed matter systems (for example in models for polymers, high temperature superconductors, etc) to high energy physics, most notably as effective models for QCD, like the Nambu–Jona-Lasinio (NJL) model [2] and its variants, including the Gross–Neveu (GN) model [3]. These theories are typically employed in the study of chiral transition, either for the discrete form of the symmetry, $\psi \rightarrow \gamma_5\psi$, or in the continuous form, $\psi \rightarrow \exp(i\alpha\gamma_5)\psi$. The general interest is to understand how the chiral transition pattern is affected by external control parameters such as the temperature (T) and the chemical potential (μ). It is also well known that, apart from these control parameters, the presence of an external magnetic field may impact significantly on the phase transition patterns.

So far we have a reasonable understanding of how chiral symmetry is affected by T , μ as well as by the presence of a magnetic field B . Mostly, this understanding is acquired at the mean-field level [4] for both the GN and the NJL models. Recently, the understanding of how an external B field affects the symmetry aspects of these four-fermion theories turned out to be a question of general interest for the following reasons. First, the interaction of fermions with an external B field is expected to be associated with phenomena such as the metal-to-insulating phase transition in semiconductors [5], quantum Hall effects [6] and the transport properties in superconductors [7], just to mention a few phenomena in the context of condensed matter physics, while in the high energy physics domain the effects of a

*Electronic address: jlkneur@univ-montp2.fr

†Electronic address: marcus@fsc.ufsc.br

‡Electronic address: rudnei@uerj.br

magnetic background is important to the physics of compact stellar objects [8], heavy-ion collisions at the Relativistic Heavy Ion Collider and at the LHC [9] and in the physics of the early universe [10], which are situations where high intensity fields, $B \sim 10^{17} - 10^{20} G$, are expected to be present or produced (for a recent review, see e.g. Ref. [11] and references therein).

Of topical interest is to understand how a magnetic field will affect phase transitions, since they can induce dynamical symmetry breaking, or magnetic catalysis [12, 13]. Within fermionic systems¹, magnetic catalysis refers to the generation of a mass gap for the fermions at any finite interaction strength, leading explicitly to chiral symmetry breaking².

In this work, we apply the optimized perturbation theory (OPT) [15] (see Ref. [16] for early works on this subject) to the GN model in 2+1 dimensions and investigate how dynamical chiral symmetry breaking (CSB) is affected by the presence of a magnetic field, comparing our results with those obtained in the large- N (LN) approximation, which is equivalent to the well known mean field approximation (MFA). The OPT has already established itself as a powerful method in dealing with critical theories. For example, in the Bose–Einstein condensation case this method and its different variations have provided some of the most precise analytical results for the shift in the critical temperature for weakly interacting homogeneous Bose gases [17]. Other applications to condensed matter situations include a precise evaluation of the critical density for polyacetylene [18]. Also, when extended by hard-thermal loops, the method was successful in predicting QCD thermodynamical properties at the three-loop level [19]. Improved by the renormalization group, and inspired by similar properties [20] in the Gross–Neveu model, a variation of the OPT has been recently used in the evaluation of $\Lambda_{\text{MS}}^{\text{QCD}}$ [21] and α_S [22], where the stability and convergence at higher orders of this renormalization group OPT form was demonstrated. For the present application it is worth mentioning that the OPT was instrumental in the determination of the phase diagram of the massless GN model in 2+1 dimensions at finite T and μ in the absence of magnetic fields [23]. In this case, the LN approximation predicts that the whole $T - \mu$ plane is dominated by a second-order phase transition, except at $T = 0$, where a first-order phase transition is predicted to occur. But, Monte–Carlo numerical simulations [24, 25] have indicated that a first-order transition line should appear at the low- T and high- μ region, terminating in a tricritical point at intermediate values of T and μ . However, no precise location for this tricritical point was possible to be given. This situation has been changed when the complete phase diagram for the model was studied in the context of the OPT method and the precise location of the tricritical point determined for any value of N [26]. The two-flavor NJL model in 3 + 1 dimensions with physical quark masses has also been treated with the OPT at finite T and μ in the absence of magnetic fields [27]. The main outcome was that the $1/N$ corrections brought in by this approximation generate the effects of a repulsive vector channel (absent in the original Lagrangian), which weakens the first-order transition line and locates the critical end point at temperature values that are smaller than the ones predicted by the LN approximation. A detailed discussion about the physical nature of the OPT $1/N$ corrections in the simplified Abelian NJL model context was recently carried out in Ref. [28].

In the massless GN model, the LN approximation predicts that the critical temperature, which signals that chiral symmetry has been restored through a second-order phase transition, increases with B at vanishing fermionic densities. However, although the functional renormalization group technique [29] has been recently applied to analyze magnetic catalysis at zero temperatures and densities, we are not aware of evaluations that go beyond mean field at finite T , μ and B in the context of the GN model in 2 + 1 dimensions. In the present work we show that at $\mu = 0$ the results obtained with the LN method and the OPT agree from the qualitative point of view. Namely, magnetic catalysis still takes place and the critical temperature rises with B . However, at the other extreme of the phase diagram, when $T = 0$ and $\mu \neq 0$, we find that the OPT and the LN predict different qualitative and quantitative behaviors as far as the coexistence chemical potential μ_c is concerned. The differences are more pronounced for negative couplings ($\lambda < 0$), where the OPT reproduces the phenomenon of inverse magnetic catalysis (IMC) [30], which predicts the decrease of μ_c with increasing B , even at large magnitude of magnetic fields. Other qualitative differences happen in the region spanned by intermediate to high chemical potentials, where the OPT adds terms of the form $\lambda \langle \psi^+ \psi \rangle^2 / N$ to the free energy, while only scalar condensates ($\langle \bar{\psi} \psi \rangle$) are considered within the LN approximation. Then, depending on the sign of the four-fermion coupling λ and for sufficiently large values of the magnetic field, we observe the weakening ($\lambda < 0$) or the enhancement ($\lambda > 0$) of the entire CSB region in the magnetized fermionic system. The OPT also predicts that the value of μ_c (at $T = 0$) can be smaller than the tricritical point value (μ_{tric}), producing an important change in the shape of the phase diagram as compared to the one generated by taking $N \rightarrow \infty$. Finally,

¹ Though magnetic catalysis is usually related to the physics of fermionic systems, it can also work for bosonic scalar fields as well [14], by enhancing the ordered phase in the presence of an external magnetic field.

² Chiral symmetry breaking can also arise in free fermionic systems as a consequence of the *quantum anomalies* although, in this case, it does not produce a mass term for the fermions, whose spectrum remains unchanged [6].

we also discuss the possibility that the order parameter value suffers more than one discontinuity as μ increases when $T = 0$ and B is small. Being observed by both approximations when $\lambda < 0$, this feature is not an artifact of the LN approximation and can be easily explained by a close examination of the filling of the Landau levels.

This paper is organized as follows. In the next section we briefly review the planar GN four-fermion model within the OPT formalism. In Sec. III we obtain the effective potential (or free energy density), at first nontrivial order, which is adequate to treat a hot, dense and magnetized planar four-fermion system. Next, in Sec. IV we discuss how finite N effects affect thermodynamical quantities such as the order parameter, the critical quantities and the overall shape of the phase diagram when a magnetic field is present. The results obtained from the OPT are contrasted with those produced by the LN approximation in all the cases we have analyzed. Finally, in Sec. V, we give our concluding remarks. Two appendices are also included to show and clarify some technical aspects.

II. GN MODEL IN AN EXTERNAL CONSTANT MAGNETIC FIELD IN THE OPT FORMALISM

In the presence of an external electromagnetic potential A_μ , the GN model with fermions with N flavors, ψ_k ($k = 1, \dots, N$), is described by the Lagrangian density [3]

$$\mathcal{L} = \bar{\psi}_k (i \not{\partial} - e \not{A}) \psi_k - m_f \bar{\psi}_k \psi_k + \frac{g^2}{2} (\bar{\psi}_k \psi_k)^2. \quad (2.1)$$

Note that a summation over fermionic species is implicit in the above equation with, e.g., $\bar{\psi}_k \psi_k = \sum_{k=1}^N \bar{\psi}_k \psi_k$. When $m_f = 0$, which is the case considered by us here, the theory is invariant under the discrete chiral symmetry (CS) transformation

$$\psi \rightarrow \gamma_5 \psi, \quad (2.2)$$

with the gamma matrices being 4×4 matrices and we follow the representation given, e.g., in Ref. [1] for fermions in 2+1 dimensions³. A constant magnetic field B along the z direction, perpendicular to the plane of the system defined by Eq. (2.1), can be considered by choosing a gauge where the external electromagnetic potential is given, for example, by $A_\mu = (0, 0, Bx, 0)$.

The LN limit (or MFA) of the model Eq. (2.1) is defined by considering the four-fermion interaction as $g^2 = \lambda/N$ and taking $N \rightarrow \infty$, while keeping λ fixed (see, e.g., Ref. [32]). In the following we will study the model of Eq. (2.1) beyond the simplest MFA/LN approximation by employing the OPT method.

Within the OPT framework one makes use of a linear interpolation on the original model in terms of a fictitious parameter, δ (used only for bookkeeping purposes), which allows for further expansions [15]. Then, following e.g. Refs. [23, 33], the interpolated GN four-fermion theory can be expressed as

$$\mathcal{L}_\delta(\psi, \bar{\psi}) = \bar{\psi}_k (i \not{\partial} - e \not{A}) \psi_k - (1 - \delta) \eta \bar{\psi}_k \psi_k + \delta \frac{\lambda}{2N} (\bar{\psi}_k \psi_k)^2. \quad (2.3)$$

Note that at $\delta = 0$ we have a theory of free fermions, while at $\delta = 1$ we recover the original theory. We can now rewrite the four-fermion interaction in Eq. (2.3) by introducing an auxiliary scalar field σ in the usual way [32], such that Eq. (2.3) becomes:

$$\mathcal{L}_\delta = \bar{\psi}_k (i \not{\partial} - e \not{A}) \psi_k - \delta \sigma \bar{\psi}_k \psi_k - (1 - \delta) \eta \bar{\psi}_k \psi_k - \frac{\delta N}{2\lambda} \sigma^2, \quad (2.4)$$

where σ and the chiral operator are related, from the saddle-point solution for σ , by $\sigma = -(\lambda/N) \bar{\psi}_k \psi_k$. Renormalization issues do not arise at the level of the approximation considered in the present application, but the interested reader can find a comprehensive discussion in the context of the OPT method in Ref. [23], for example.

Any quantity computed from the above interpolated Lagrangian density (2.4), at some finite order in δ , is dependent on the arbitrary mass parameter η , which also serves as an infrared regulator. Then, after the formal mathematical

³ Note that chiral symmetry breaking in 2+1 dimensions requires fermion fields with four-component spinors so that the gamma matrices are represented by 4×4 Dirac matrices (see e.g. Ref. [31] for details), as we implicitly consider in this work.

manipulations associated with the evaluation of the relevant Green functions, one must fix the arbitrary η in a judicious way. Here, as in most of the previous works on the OPT method (see, e.g., Refs. [23, 33, 34]), η is fixed by using the principle of minimal sensitivity (PMS). Within the PMS procedure one requires that a physical quantity $\Phi^{(k)}$, that is calculated perturbatively to some k -th order in δ , be evaluated at the point where it is less sensitive to this mass parameter. This criterion then translates into the variational relation [35]

$$\left. \frac{d\Phi^{(k)}}{d\eta} \right|_{\bar{\eta}, \delta=1} = 0. \quad (2.5)$$

The optimum value $\bar{\eta}$ that satisfies Eq. (2.5) must be a function of the original parameters, including the couplings, thus generating in that sense nonperturbative dependences in the coupling and other parameters of the model.

III. EFFECTIVE POTENTIAL FOR THE INTERPOLATED THEORY

Following, e.g., Ref. [23], the effective potential (or free-energy density) for a constant background scalar field, σ_c , at first order in the OPT approximation is given by

$$\frac{1}{N} V_{\text{eff}, \delta^1}(\sigma_c, \eta) = \delta \frac{\sigma_c^2}{2\lambda} + i \int_p \text{tr} \ln(\not{P} - \eta) + \delta i \int_p \text{tr} \frac{\eta - \sigma_c}{\not{P} - \eta + i\epsilon} + \frac{1}{N} \Delta V_{\text{eff}, \delta^1}, \quad (3.1)$$

where $\Delta V_{\text{eff}, \delta^1}/N$ brings the first $1/N$ corrections to the effective potential. This contribution is explicitly given by

$$\frac{1}{N} \Delta V_{\text{eff}, \delta^1} = -\frac{i}{2N} \int_p \text{tr} \left[\frac{\Sigma_{\delta^1}(\eta)}{\not{P} - \eta + i\epsilon} \right], \quad (3.2)$$

where $\Sigma_{\delta^1}(\eta)$ is the $\mathcal{O}(\delta)$ contribution to the fermion self-energy,

$$\Sigma_{\delta^1}(\eta) = -\delta \frac{\lambda}{N} i \int_q \frac{1}{\not{Q} - \eta + i\epsilon}. \quad (3.3)$$

The traces in Eqs. (3.1) and (3.2) are taken over Dirac's matrices only (a factor of -1 , corresponding to a closed fermionic loop, has already been taken into account [36] in the above expressions). After taking the traces over the Dirac's matrices and rearranging the terms, Eq. (3.1) can be written as

$$\begin{aligned} \frac{1}{N} V_{\text{eff}, \delta^1}(\sigma_c, \eta) &= \delta \frac{\sigma_c^2}{2\lambda} + 2i \int_p \ln(P^2 - \eta^2) + \delta 4i \int_p \frac{\eta(\eta - \sigma_c)}{P^2 - \eta^2 + i\epsilon} \\ &+ \delta \frac{2\lambda}{N} \eta^2 \left[i \int_p \frac{1}{P^2 - \eta^2 + i\epsilon} \right]^2 + \delta \frac{2\lambda}{N} \left[i \int_p \frac{P_0}{P^2 - \eta^2 + i\epsilon} \right]^2. \end{aligned} \quad (3.4)$$

In the above expressions we are using the notation for the momentum integrations in $(2+1)$ dimensions, at finite temperature and chemical potential and in the presence of a constant magnetic field. Expressed in terms of sums over discrete Matsubara's frequencies and Landau levels (LLs) the integral measure is given by

$$\int_p = \int \frac{d^3p}{(2\pi)^3} \equiv iT \sum_{\nu=-\infty}^{\infty} \frac{eB}{2\pi} \sum_{j=0}^{\infty} \frac{2 - \delta_{j,0}}{2}, \quad (3.5)$$

where $\omega_\nu = (2\nu + 1)\pi T$, with $\nu = 0, \pm 1, \pm 2, \dots$, are the Matsubara frequencies for fermions, with T the temperature. The sum over j are over the Landau levels (LL), with a density of states $eB/(2\pi)$. The time and space components of the momentum are $p_0 \rightarrow i(\omega_\nu - i\mu)$, where μ is the chemical potential, while $\mathbf{p}^2 \rightarrow 2jeB$ gives the (square of the) Landau energy levels, with the factor $(2 - \delta_{j,0})$ accounting for the degeneracy of the $j \geq 1$ Landau levels [12, 13].

Then, using Eq.(3.5) and performing the sums over the Matsubara frequencies, the explicit expression for the effective potential (3.4) can be obtained. It can be written in the form

$$\begin{aligned} \frac{1}{N} V_{\text{eff}, \delta^1}(\sigma_c, \eta, B, T, \mu) &= \delta \frac{\sigma_c^2}{2\lambda} + 2I_1(\eta, B, T, \mu) + 4\delta \eta(\eta - \sigma_c)I_2(\eta, B, T, \mu) \\ &+ 2\delta \frac{\lambda}{N} [\eta^2 I_2^2(\eta, B, T, \mu) + I_3^2(\eta, B, T, \mu)] , \end{aligned} \quad (3.6)$$

where $I_i(\eta, B, T, \mu)$, $i = 1, 2, 3$, are given by (see also Appendix A)

$$I_1(\eta, B, T, \mu) = \frac{eB\eta}{4\pi} - \frac{(2eB)^{3/2}}{4\pi} \zeta\left(-\frac{1}{2}, \frac{\eta^2}{2eB}\right) - \frac{eBT}{4\pi} \sum_{j=0}^{\infty} \alpha_j \left\{ \ln[1 + e^{-(E_j+\mu)/T}] + \ln[1 + e^{-(E_j-\mu)/T}] \right\} , \quad (3.7)$$

$$I_2(\eta, B, T, \mu) = -\frac{eB}{8\pi\eta} + (2eB)^{1/2} \frac{1}{8\pi} \zeta\left(\frac{1}{2}, \frac{\eta^2}{2eB}\right) - \frac{eB}{8\pi} \sum_{j=0}^{\infty} \alpha_j \left\{ \frac{1}{E_j[1 + e^{(E_j+\mu)/T}]} + \frac{1}{E_j[1 + e^{(E_j-\mu)/T}]} \right\} , \quad (3.8)$$

$$I_3(\eta, B, T, \mu) = \frac{eB}{8\pi} \sum_{j=0}^{\infty} \alpha_j \left[\frac{1}{1 + e^{(E_j-\mu)/T}} - \frac{1}{1 + e^{(E_j+\mu)/T}} \right] , \quad (3.9)$$

where $E_j = \sqrt{2jeB + \eta^2}$, $\alpha_j = 2 - \delta_{j,0}$ and $\zeta(s, a)$ is the Hurwitz zeta function [37],

$$\zeta(s, a) = \sum_{k=0}^{\infty} \frac{1}{(k+a)^s} . \quad (3.10)$$

It can be easily shown from Eq. (3.6) that in the large- N limit we reobtain the standard expression for the effective potential for this model, as found, e.g., in the seminal papers [12, 13].

It is also useful to realize that Eqs. (3.8) and (3.9) can be both expressed in terms of Eq. (3.7):

$$I_2 = -\frac{1}{2\eta} \frac{\partial}{\partial \eta} I_1 , \quad (3.11)$$

$$I_3 = -\frac{1}{2} \frac{\partial}{\partial \mu} I_1 . \quad (3.12)$$

Finally, let us analyze the physical meaning of the OPT $1/N$ corrections displayed by Eq. (3.6). By recalling that at one-loop order one can write the fermion number density as

$$\langle \psi^+ \psi \rangle = 2NI_3 , \quad (3.13)$$

and the scalar condensate as

$$\langle \bar{\psi} \psi \rangle = -2N\eta I_2 , \quad (3.14)$$

then, it is easy to see that Eq. (3.2) becomes

$$\Delta V_{\text{eff}, \delta^1} = \frac{g^2}{2N} [\langle \psi^+ \psi \rangle^2 + \langle \bar{\psi} \psi \rangle^2] , \quad (3.15)$$

where we have used $\lambda/N \equiv g^2$. Therefore, contrary to the LN approximation, the OPT brings in a $1/N$ suppressed term that only contributes at finite densities. Thus, one may expect some important differences to arise as this term becomes more important at increasing μ values [28].

As an aside, concerning the values of the coupling λ leading to chiral symmetry breaking, note that we can define a renormalization condition for the coupling as $1/\lambda_R = 1/\lambda - 1/\lambda_c$, with $1/\lambda_c = 4 \int d^d p / (2\pi)^d 1/p^2$. In terms of a

cutoff regularization, in $2 < D < 4$ dimensions λ_c defines (for vanishing magnetic field) a critical value for which chiral symmetry breaking can happen [13], such that for $\lambda > \lambda_c$ (i.e., corresponding to $\lambda_R < 0$) the model can be in the broken phase of the discrete chiral symmetry, while for $0 \leq \lambda \leq \lambda_c$ (i.e., corresponding to $\lambda_R \geq 0$), there is no chiral symmetry breaking. Some authors prefer to work directly in terms of the bare coupling λ (like in Ref. [13]), while others prefer to work in terms of the redefined coupling λ_R (like, for example, in Refs. [12, 38]). The latter is necessarily the case when working directly in terms of dimensional regularization, as we consider here, since then the above integral vanishes by definition, and $\lambda = \lambda_R$. Note also that within dimensional regularization there are no additional divergences in the OPT case (see, e.g., Ref. [23] for more details).

IV. OPTIMIZATION AND NUMERICAL RESULTS BEYOND LARGE N

The optimization of the effective potential, Eq. (3.6), is easily implemented by applying the PMS condition, Eq. (2.5), to V_{eff} . Let us initially apply the PMS to the most general order- δ effective potential, which is given by Eq. (3.4). This exercise will help the reader to visualize the way the OPT-PMS resums the perturbative series. Setting $\delta = 1$ and applying the PMS to Eq. (3.4), we obtain that

$$\left\{ \left[\eta - \sigma_c + \eta \frac{\lambda}{N} \left(i \int_p \frac{1}{P^2 - \eta^2 + i\epsilon} \right) \right] \left(1 + \eta \frac{d}{d\eta} \right) \left[i \int_p \frac{1}{P^2 - \eta^2 + i\epsilon} \right] + \frac{\lambda}{N} \left(i \int_p \frac{P_0}{P^2 - \eta^2 + i\epsilon} \right) \frac{d}{d\eta} \left(i \int_p \frac{P_0}{P^2 - \eta^2 + i\epsilon} \right) \right\} \Big|_{\eta=\bar{\eta}} = 0. \quad (4.1)$$

From the result given by Eq. (3.9), the last term of Eq. (4.1) only survives when $\mu \neq 0$. In the case $\mu = 0$, Eq. (4.1) factorizes in a nice way, which allows us to understand the way the OPT-PMS procedure resums the series producing nonperturbative results. Then, when $\mu = 0$, and using Eq. (3.3), the OPT-PMS Eq. (4.1) factorizes to

$$[\bar{\eta} - \sigma_c - \Sigma_{\delta^1}(\bar{\eta})|_{\mu=0}] \left(1 + \bar{\eta} \frac{\partial}{\partial \bar{\eta}} \right) \left[i \int_p \frac{1}{P^2 - \bar{\eta}^2 + i\epsilon} \right] = 0, \quad (4.2)$$

leading to the self-consistent relation ⁴

$$\bar{\eta} = \sigma_c + \Sigma_{\delta^1}(\bar{\eta})|_{\mu=0}, \quad (4.3)$$

which is valid for any temperature and number of space-time dimensions provided that $\mu = 0$. In this way the OPT fermionic loops get contributions containing σ_c as well as a rainbow (exchange) type of self-energy terms, given by Eq. (3.3). Note that when $N \rightarrow \infty$, $\bar{\eta} = \sigma_c$ and the large- N result is exactly reproduced [33].

When $\mu \neq 0$, we can consider Eq. (4.1) in order to get the general result in terms of the I_i ($i = 1, 2, 3$) terms defined in the previous section. Alternatively, using Eqs. (3.11) and (3.12) we obtain that $\bar{\eta}$ is given by the solution of

$$\bar{\eta} = \sigma_c + \frac{\lambda}{2N} \left[\frac{\partial I_1}{\partial \eta} + \frac{\left(\frac{\partial I_1}{\partial \mu} \right) \left(\frac{\partial^2 I_1}{\partial \eta \partial \mu} \right)}{\frac{\partial^2 I_1}{\partial \eta^2}} \right] \Big|_{\eta=\bar{\eta}}. \quad (4.4)$$

Again, we see from Eq. (4.4) that as $N \rightarrow \infty$, the large- N result $\bar{\eta} = \sigma_c$ is recovered.

The PMS equation (4.4) is to be solved together with the one defining the vacuum expectation value for the background field σ_c ,

$$\frac{\partial V_{\text{eff}}}{\partial \sigma_c} \Big|_{\sigma_c=\bar{\sigma}, \eta=\bar{\eta}} = 0 \quad \Rightarrow \quad \bar{\sigma} = 4\lambda \bar{\eta} I_2. \quad (4.5)$$

⁴ The second solution is usually discarded on the grounds that it is coupling independent and, moreover, does not reproduce the LN “exact” result if one considers the OPT in the $N \rightarrow \infty$ limit.

We now have all the necessary tools to investigate all the possible cases when considering a finite constant magnetic field applied to the system. As a ballpark estimate we shall consider magnetic fields ranging from $eB = 0$ to $eB = 20\Lambda^2$, since the gap energy is about Λ within this model. This choice is reasonable since, keeping in mind possible applications to condensed matter systems for example, typically, the gap energy lies within the range 10 – 100 meV and if, for example, one considers the lower gap value $\Lambda \sim 10$ meV then $eB = 20\Lambda^2 \sim 3$ Teslas, which is a realistic value within current planar condensed matter systems⁵. Finally, we set $N = 2$, since this is the relevant value as far as planar condensed matter systems (like high-temperature superconductor films or graphene) are concerned.

A. $T = 0$ and $\mu = 0$ case

Let us preliminarily examine the case of zero temperature and zero chemical potential, $T = \mu = 0$. An important effect here is that of magnetic catalysis [12, 13], which we next investigate in order to analyze how this phenomenon is affected by the nonperturbative inclusion of finite N corrections through the OPT. From Eq. (3.6) for the effective potential and upon using the results (A14), (A15), and (A16) obtained in the appendix, we have that

$$\begin{aligned} \frac{1}{N} V_{\text{eff}, \delta^1}(\sigma_c, \eta, B, T = 0, \mu = 0) &= \delta \frac{\sigma_c^2}{2\lambda} + \frac{eB\eta}{2\pi} - \frac{(2eB)^{3/2}}{2\pi} \zeta\left(-\frac{1}{2}, \frac{\eta^2}{2eB}\right) \\ &- \delta \frac{\eta(\eta - \sigma_c)}{2\pi} \left[\frac{eB}{\eta} - (2eB)^{1/2} \zeta\left(\frac{1}{2}, \frac{\eta^2}{2eB}\right) \right] \\ &+ \delta \frac{\lambda\eta^2}{32\pi^2 N} \left[\frac{eB}{\eta} - (2eB)^{1/2} \zeta\left(\frac{1}{2}, \frac{\eta^2}{2eB}\right) \right]^2. \end{aligned} \quad (4.6)$$

Then, from Eq. (4.4), we obtain the self-consistent relation to be evaluated for $\bar{\eta}$:

$$\bar{\eta} = \sigma_c + \frac{\lambda}{8\pi N} \left[eB - \bar{\eta} (2eB)^{1/2} \zeta\left(\frac{1}{2}, \frac{\bar{\eta}^2}{2eB}\right) \right]. \quad (4.7)$$

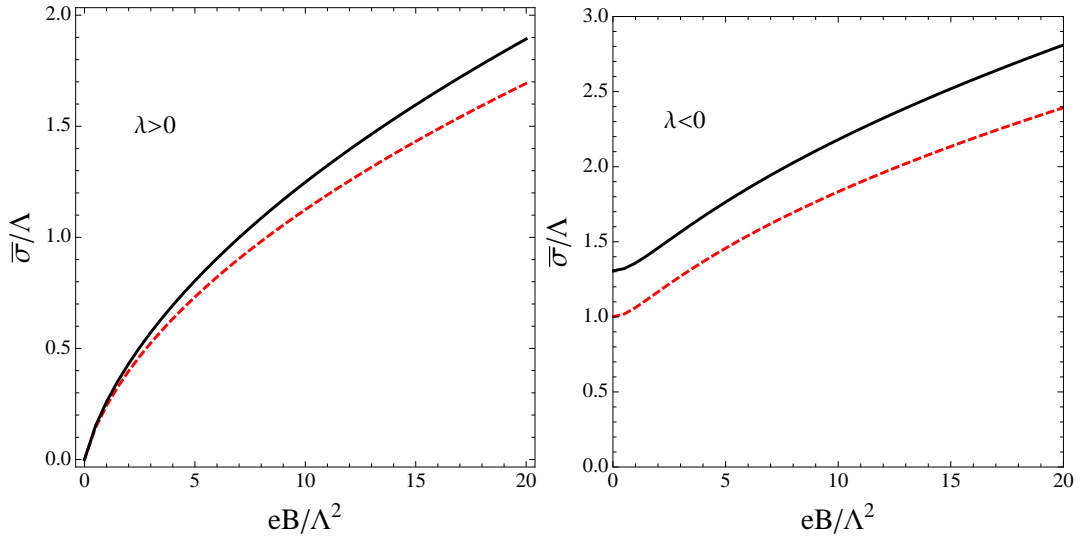


FIG. 1: The order parameter $\bar{\sigma}$, as a function of eB and for $N = 2$, illustrating the phenomenon of magnetic catalysis at $T = 0$ and $\mu = 0$. The dashed line is the large N result, and the continuous line represents the OPT result. The left panel shows the case $\lambda > 0$, illustrating how a finite magnetic field induces CSB. The right panel shows the situation for the $\lambda < 0$ case, when CSB occurs even at $B = 0$.

⁵ When converting our results to condensed matter systems, note that one should also include explicitly the Fermi velocity in the expressions [18].

By extremizing the effective potential (4.6) with respect to σ_c , setting $\delta = 1$ and using the optimal $\bar{\eta}$, one finds that the order parameter satisfies

$$\frac{\bar{\sigma}}{\lambda} = -\frac{1}{2\pi} \left[eB - \bar{\eta} (2eB)^{1/2} \zeta \left(\frac{1}{2}, \frac{\bar{\eta}^2}{2eB} \right) \right]. \quad (4.8)$$

Then, comparing the above equation with Eq. (4.7), one is lead to the relation

$$\bar{\eta} = \bar{\sigma} \mathcal{F}(N), \quad (4.9)$$

where

$$\mathcal{F}(N) = 1 - \frac{1}{4N}. \quad (4.10)$$

By using Eq. (4.9) in Eq. (4.8), we obtain

$$\frac{\bar{\sigma}}{\lambda} = -\frac{eB}{2\pi} + \frac{\bar{\sigma} \mathcal{F}(N)}{2\pi} (2eB)^{1/2} \zeta \left(\frac{1}{2}, \frac{\bar{\sigma}^2 \mathcal{F}(N)^2}{2eB} \right). \quad (4.11)$$

Chiral symmetry breaking can now be investigated by looking at the case $\lambda > 0$, in which CSB does not occur when $B = 0$, and also the case $\lambda < 0$, where dynamical CSB occurs even at $B = 0$. All quantities will be expressed in terms of the scale $\Lambda = \pi/|\lambda|$, which is the value of the chiral condensate $\bar{\sigma}$ in the LN case. Our numerical results are compared to the ones given by the LN approximation in Fig. 1 for $N = 2$. We note that when either $\lambda > 0$ or $\lambda < 0$, the magnetic catalysis is enhanced by the finite N contributions that the OPT-PMS method brings, as Fig 1 shows.

B. $T \neq 0$ and $\mu = 0$ case

As in the previous subsection, we start with Eq. (3.6) for the free energy density and use the results (A11), (A12) and (A13) to write

$$\begin{aligned} \frac{1}{N} V_{\text{eff}, \delta^1}(\sigma_c, \eta, B, T, \mu = 0) &= \delta \frac{\sigma_c^2}{2\lambda} + 2 \left[\frac{eB\eta}{4\pi} - \frac{(2eB)^{3/2}}{4\pi} \zeta \left(-\frac{1}{2}, \frac{\eta^2}{2eB} \right) - \frac{eBT}{2\pi} \sum_{j=0}^{\infty} \alpha_j \ln \left(1 + e^{-E_j/T} \right) \right] \\ &+ 4\delta \eta (\eta - \sigma_c) \left[-\frac{eB}{8\pi\eta} + \frac{(2eB)^{1/2}}{8\pi} \zeta \left(\frac{1}{2}, \frac{\eta^2}{2eB} \right) - \frac{eB}{4\pi} \sum_{j=0}^{\infty} \alpha_j \frac{1}{E_j (1 + e^{E_j/T})} \right] \\ &+ 2\delta \frac{\lambda}{N} \eta^2 \left[-\frac{eB}{8\pi\eta} + \frac{(2eB)^{1/2}}{8\pi} \zeta \left(\frac{1}{2}, \frac{\eta^2}{2eB} \right) - \frac{eB}{4\pi} \sum_{j=0}^{\infty} \alpha_j \frac{1}{E_j [1 + e^{E_j/T}]} \right]^2, \quad (4.12) \end{aligned}$$

The expression for the order parameter $\bar{\sigma}$, equivalent to Eq. (4.11) in the case of $T = 0$, now reads

$$\frac{\bar{\sigma}}{\lambda} = -\frac{eB}{2\pi} + \frac{\bar{\sigma} \mathcal{F}(N)}{2\pi} (2eB)^{1/2} \zeta \left(\frac{1}{2}, \frac{\bar{\sigma}^2 \mathcal{F}(N)^2}{2eB} \right) - \frac{eB}{4\pi} \sum_{j=0}^{\infty} \alpha_j \frac{1}{E_j(\bar{\sigma}) [1 + e^{E_j(\bar{\sigma})/T}]}, \quad (4.13)$$

where $E_j(\bar{\sigma}) = \sqrt{2jeB + \bar{\sigma}^2 \mathcal{F}^2(N)}$ and we have used Eq. (4.9), which still holds at $T \neq 0$ and $\mu = 0$.

The thermal behavior for the order parameter, $\bar{\sigma}(T)$, is shown in Fig. 2 for $eB = 0$ and for $eB = 20\Lambda^2$. In both cases the transition is of the second kind and, as expected, in the later case the symmetry restoration happens at a higher T_c . Figure 3 shows how the critical temperature increases with B , which is expected since $\bar{\sigma}$ increases with B and $T_c \sim \bar{\sigma}$. In this model even a strong magnetic field (e.g., $eB \sim 30\Lambda^2$) is not able to change the character of the phase transition. It is interesting to note that for $\lambda > 0$ the OPT predicts that the order parameter assumes higher values than the ones predicted by the LN approximation as B increases as the left panel of Fig. 1 suggests. However, despite the fact that chiral symmetry seems to be more severely broken within the OPT framework, the left panel of Fig. 3 shows that this symmetry will be restored at smaller critical temperatures than those predicted by the LN approximation.

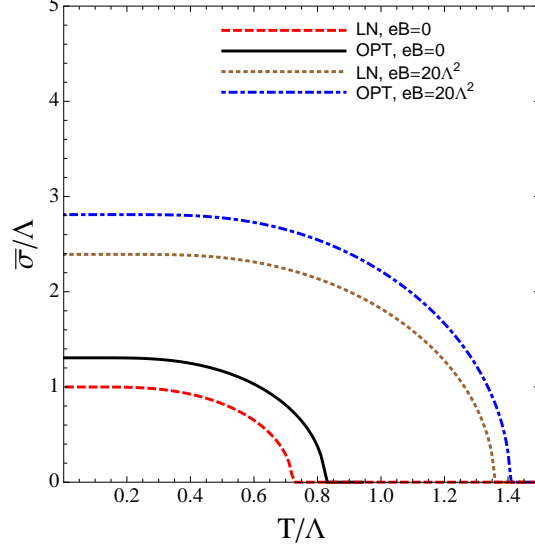


FIG. 2: The order parameter, $\bar{\sigma}/\Lambda$, as a function of T/Λ for $N = 2$ at $\mu = 0$ for $B = 0$ and $eB = 20\Lambda^2$. The dashed lines represent the large- N result and the continuous lines represents the OPT result. The figure illustrates a transition of the second kind for all the four cases.

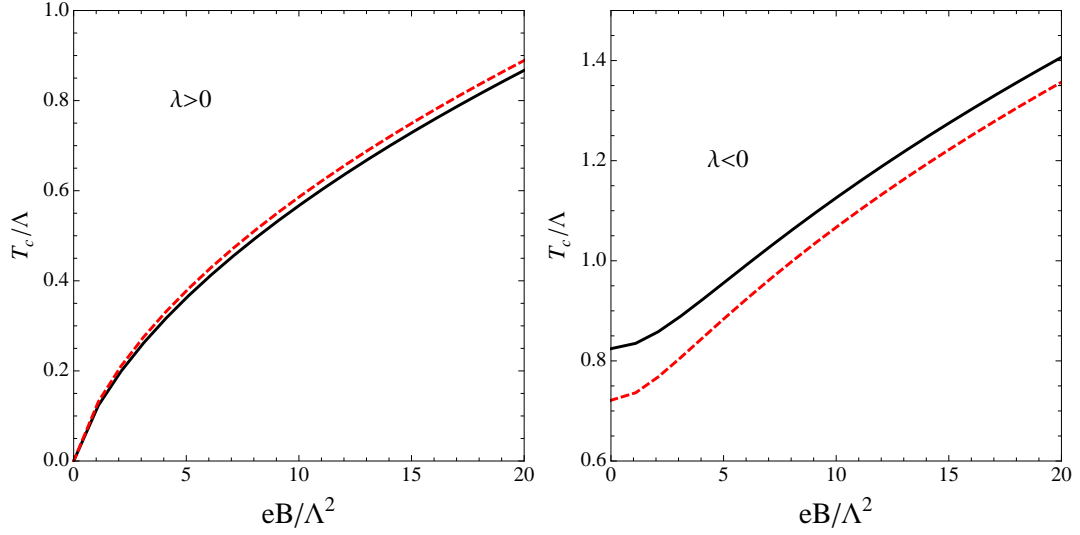


FIG. 3: The critical temperature, T_c/Λ , as a function of eB/Λ^2 for $N = 2$ and $\mu = 0$. The dashed lines represent the large- N result and the continuous lines represent the OPT result. The left panel is for $\lambda > 0$ and the right panel for $\lambda < 0$.

C. $T = 0$ and $\mu \neq 0$ case

The next case we analyze is when $T = 0$ and $\mu \neq 0$, which is relevant, for example, when analyzing charge asymmetries [39]. The OPT first-order result for the effective potential in this case becomes

$$\begin{aligned} \frac{1}{N} V_{\text{eff}, \delta^1}(\sigma_c, \eta, B, T = 0, \mu) &= \delta \frac{\sigma_c^2}{2\lambda} + 2I_1(\eta, B, T = 0, \mu) + 4\delta \eta(\eta - \sigma_c)I_2(\eta, B, T = 0, \mu) \\ &+ 2\delta \frac{\lambda}{N} [\eta^2 I_2^2(\eta, B, T = 0, \mu) + I_3^2(\eta, B, T = 0, \mu)] , \end{aligned} \quad (4.14)$$

where the expressions for $I_i(\eta, B, T = 0, \mu)$, $i = 1, 2, 3$, are again as those given in the Appendix A by Eqs. (A8), (A9) and (A10), respectively.

Then, using Eq. (4.5) one can write the order parameter as

$$\bar{\sigma} \equiv 4\lambda I_2(\eta, B, T = 0, \mu) = 4\lambda\bar{\eta} \left[-\frac{eB}{8\pi\eta} + \frac{(2eB)^{1/2}}{8\pi} \zeta\left(\frac{1}{2}, \frac{\eta^2}{2eB}\right) - \frac{eB}{8\pi} \sum_{j=0}^{\frac{\mu^2 - \eta^2}{2eB}} \alpha_j \frac{1}{E_j} \theta(\mu - \eta) \right], \quad (4.15)$$

while the PMS equation for $\mu \neq 0$ now takes the more general form of Eq. (4.4), which after some algebra can be expressed for $T = 0$ as

$$\bar{\eta} = \bar{\sigma}\mathcal{F}(N) + \frac{\lambda}{4\pi N} \eta \left[\frac{I_3(\eta, B, T = 0, \mu)}{(1 + \eta \frac{\partial}{\partial \eta}) I_2(\eta, B, T = 0, \mu)} \right], \quad (4.16)$$

where the relevant expressions for I_i at $T = 0$ are given in Appendix A in Eqs. (A9)-(A10) and the OPT corrections for $\mu \neq 0$ to the simpler relation in Eq. (4.9), $\bar{\eta} = \bar{\sigma}\mathcal{F}(N)$, are explicit from the second term. In Eq. (4.16) we have used

$$\frac{\partial}{\partial \eta} I_3(\eta, B, T, \mu)|_{T \rightarrow 0} = -\frac{\eta}{4\pi} \quad (4.17)$$

which is independent of B ⁶. Note, however, that the second term in (4.16) being suppressed by $(4\pi N)^{-1}$ gives a reasonably small correction, moreover only nonvanishing for $\mu > \eta$ due to the step function in I_3 Eq. (A10). A legitimate approximation can thus be to use the simpler relation Eq. (4.9) *within* this correction, instead of the implicit exact η relation in (4.16), since the difference is of higher λ order, neglected anyway at the first OPT δ -order here considered. It is worth remarking that this OPT correction term, when nonvanishing, may be positive or negative depending on the sign of λ and depending on the sign of $I_2(\eta, B, T = 0, \mu)$ (while $I_3(\eta, B, T = 0, \mu) > 0$ for any B values). Thus, it may enhance η with respect to the LN result $\eta = \sigma_c$ (partly compensating the reduction from $\mathcal{F}(N) < 1$). Using the $T = 0$ analytical expression of I_2 and I_3 in Eqs. (A9) and (A10) and some properties of the Riemann–Hurwitz Zeta functions, it is not difficult to recover the $B \rightarrow 0$ limit of (4.16), having relatively simple expressions:

$$\bar{\eta}(T = 0, B \rightarrow 0) = \bar{\sigma}\mathcal{F}(N) - \frac{\lambda}{8\pi N} \frac{\eta(\mu^2 - \eta^2)\theta(\mu - \eta)}{\eta + (\mu - \eta)\theta(\mu - \eta)}, \quad (4.18)$$

which is consistent with the direct $B = 0$ calculation [23].

Here, as we shall see, chiral symmetry is restored through a first-order phase transition as in the case of the absence of the external magnetic field [23]. Therefore, we must determine the coexistence chemical potential value, μ_c , at which the discontinuous chiral symmetry transition occurs. In this case, μ_c is obtained by solving (see also discussion in the next subsection)

$$V_{\text{eff}}(\sigma_c = \bar{\sigma}, B, T = 0, \mu_c) = V_{\text{eff}}(\sigma_c = 0, B, T = 0, \mu_c). \quad (4.19)$$

Results for μ_c as a function of the magnetic field, for both cases of $\lambda < 0$ and $\lambda > 0$, in the LN and OPT cases, are shown in Fig. 4. For $eB \leq \Lambda^2$ and $\lambda < 0$, one observes the typical de Haas–van Alphen oscillations (see Appendix B) due to the filling of the Landau levels. In Fig. 5 we show the critical chemical potential $\mu_c(B)$ for $\lambda < 0$ for the region of low magnetic fields. This figure shows more clearly the typical oscillations at low magnetic fields, which are reminiscent of the de Haas–van Alphen magnetic oscillations of the magnetization. These oscillations stop after eB reaches a value such that only the lowest Landau level (LLL) has to be considered (here this happens at $eB \gtrsim \Lambda^2$).

⁶ Caution should be taken to take the derivative with respect to η of $I_3(\eta, B, T, \mu)$ before taking the $T \rightarrow 0$ limit; otherwise, the derivative of expression (A10) is ill-defined. The result (4.17) is consistent with the $B \rightarrow 0$ limit [23] for $\mu \neq 0$ of expression (4.16)

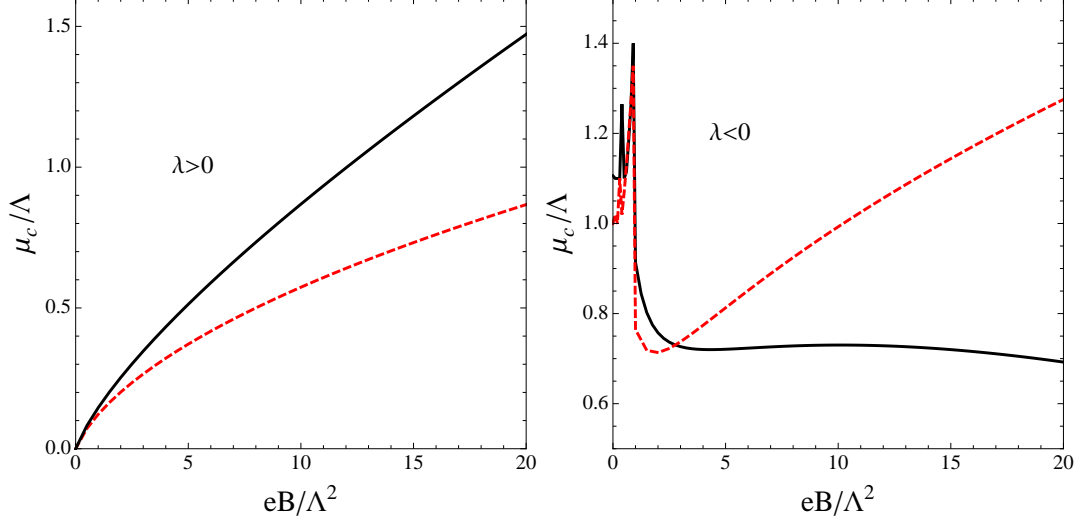


FIG. 4: The coexistence chemical potential in units of Λ as a function of eB/Λ^2 for $T = 0$. The left panel illustrates the $\lambda > 0$ case and the right panel the $\lambda < 0$ case. The OPT predicts that IMC takes place for $eB \gtrsim \Lambda^2$ when $\lambda < 0$ contrary to the large- N result which displays this phenomenon only at for $\Lambda^2 \lesssim eB \lesssim 2\Lambda^2$.

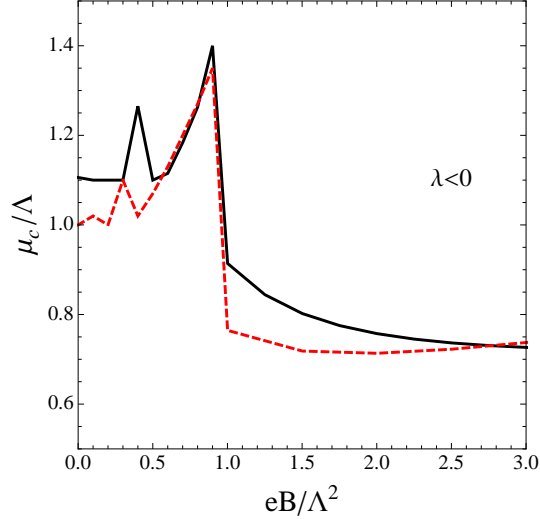


FIG. 5: de Haas-van Alphen oscillations observed when the coexistence chemical potential, μ_c/Λ , varies within the $0 < eB \lesssim \Lambda^2$ range at $T = 0$ when $\lambda < 0$.

After this point one sees a remarkable difference between the OPT and the LN approximation results. The latter predicts that μ_c decreases with eB toward a minimum and then observes a sharp increase for $eB \gtrsim 2\Lambda^2$. This LN result is in complete agreement with a MFA application to the three-flavor NJL model performed in Ref. [40] (see Ref. [41] for a detailed discussion on the first-order coexistence region). In contrast the decrease of μ_c with B in the OPT case is a manifestation of the inverse magnetic catalysis (IMC) effect, which was explained e.g. in Ref. [30] (the IMC effect was first observed in the NJL model in Ref. [42] at $T = 0$ and in Ref. [43] for the full $T - \mu - B$ case). Then, Fig. 4 shows that the OPT results are more in line with this phenomenon, since only a smooth very moderate rise of μ_c is observed to occur between $eB \simeq 5\Lambda^2$ and $eB \simeq 15\Lambda^2$, before it drops again at higher fields. This quantitative difference can be traced to the OPT $\lambda\langle\psi^\dagger\psi\rangle/N$ type of corrections, which are non-negligible in this region of high charge asymmetry. In fact the behavior can be essentially understood from a simple analytical approximation. First note that both terms of Eq. (4.19) considerably simplify. Because of $\sigma_c = 0$ the right-hand side can be written as

$$V_{\text{eff}}(\sigma_c = 0, B, T = 0, \mu) = 2I_1(0, B, 0, \mu) + 2\frac{\lambda}{N}I_3^2(0, B, 0, \mu) . \quad (4.20)$$

Also, calculating V_{eff} from Eq. (4.14) at its minimum, using the relation Eq. (4.5) between $\bar{\sigma}_c$ and η (which is valid at the minimum of the potential for any values of the other parameters), the left-hand-side of Eq. (4.19) also simplifies to

$$V_{\text{eff}}(\sigma_c, B, T = 0, \mu) = \frac{\bar{\sigma}_c^2}{2\lambda}\mathcal{F}(N) + 2I_1(\bar{\sigma}_c, B, 0, \mu) + 2\frac{\lambda}{N}I_3^2(\bar{\sigma}_c, B, 0, \mu) . \quad (4.21)$$

Moreover, the last term in Eq. (4.21) vanishes whenever $\bar{\eta} > \mu$, which is the case in most of the parameter space considered, i.e. μ_c satisfying Eq. (4.19) will be such that $\mu_c < \bar{\eta}$. The LN case can be easily recovered from the above expressions by simply neglecting the OPT correction λI_3^2 term, and taking $\mathcal{F}(N) = 1$, $\bar{\eta} = \sigma_c$ in the remaining terms. For $eB \gtrsim \Lambda^2$ only the lowest Landau level contributes to the relevant integrals, such that in this range $eB \gtrsim \Lambda^2$ Eq. (4.19) gives a relatively simple analytic (implicit) expression for μ_c in the OPT case:

$$\mu_c^{\text{OPT}} = -\mathcal{F}(N)\bar{\sigma}_c + \mathcal{F}(N)\frac{\bar{\sigma}_c^2}{eB} + 2(2eB)^{1/2} \left[\zeta\left(-1/2, \frac{\mathcal{F}^2(N)\bar{\sigma}_c^2}{2eB}\right) - \zeta(1/2) \right] + \frac{\lambda}{16\pi N eB} (eB + \mu_c^2)^2 , \quad (4.22)$$

while the corresponding expression in the LN case reads

$$\mu_c^{\text{LN}} = -\bar{\sigma}_c + \frac{\bar{\sigma}_c^2}{eB} + 2(2eB)^{1/2} \left[\zeta\left(-1/2, \frac{\bar{\sigma}_c^2}{2eB}\right) - \zeta(1/2) \right] . \quad (4.23)$$

The exact eB dependence in Eqs. (4.22) and (4.23) is rather involved, since σ_c depends nontrivially on eB , Eq. (4.15). However, for a qualitative but essentially rather accurate understanding of the behavior in Fig. 4, it is sufficient to know that $\sigma_c(eB)$ is a moderately increasing function of eB . Then the last term in Eq. (4.23) involving the ζ -functions is monotonically increasing with eB (first rapidly for moderate eB and then for large eB with a decreasing slope), so that together with the first terms it implies that $\mu_c^{\text{LN}}(eB)$ gets a minimum at a moderate eB value, and then has a steeper rise. Now, if there would only be the moderate difference $\sigma_c \rightarrow \sigma_c \mathcal{F}(N)$ from the LN to the OPT case, the OPT results would be qualitatively similar to the LN ones. In contrast, due to the last correction term in Eq. (4.22), the behavior of $\mu_c^{\text{OPT}}(eB)$ is drastically different, since for $\lambda < 0$ the last terms goes for large eB as $-(eB)/(16N)$ (the μ^2 in the last term being rapidly negligible in the relevant range $eB \gg \mu^2$), which thus prevents μ_c^{OPT} to increase fast, producing almost a plateau, before this term starts to drive μ_c to decrease for even larger values of eB . Clearly the opposite behavior happens for $\lambda > 0$, as seen in Fig. 4 (left panel). Of course, for extremely large eB values the OPT correction term will become an unreasonably large perturbative correction and not very trustable, since higher λ -order corrections are not considered at the OPT first order.

1. Intermediate transitions at low magnetic field

At low magnetic fields ($eB \lesssim \Lambda^2$) and when $\lambda < 0$, a structure of intermediate phase transitions, where the vacuum expectation value of the chiral condensate can jump discontinuously from a value $\bar{\sigma}_1 \neq 0$ to another value $\bar{\sigma}_2 \neq 0$, with $\bar{\sigma}_1 > \bar{\sigma}_2$ is possible, as shown in Fig. 6, where we show the normalized effective potential for both the LN and OPT cases, \bar{V}_N , where

$$\bar{V}_N = \frac{V_{\text{eff}}(\sigma_c, T = 0) - V_{\text{eff}}(\sigma_c = 0, T = 0)}{N\Lambda^3} . \quad (4.24)$$

Note that the multiple transitions can happen in the LN case and also in the OPT case. Therefore, this is not an artifact of the MFA. The final transition is the actual chiral phase transition, where the system jumps from $\bar{\sigma}_2 \neq 0$ to $\bar{\sigma} = 0$. In the LN case, there is an intermediate (nonchiral) transition at a value of critical chemical potential given by $\mu \simeq 0.878\Lambda$ when $eB = 0.5\Lambda^2$, while in the OPT case (for $N = 2$), this first transition happens at $\mu \simeq 1.02\Lambda$. The actual chiral phase transition happens at a larger value of chemical potential, given by $\mu \simeq 1.063\Lambda$ in the LN case and by $\mu \simeq 1.09\Lambda$ in the OPT case. In Fig. 7 we show how the chiral order parameter changes with the chemical potential, also evidencing the intermediate transitions.

An analogous structure of multiple phase transitions was first identified in Ref. [44], for which besides including the perpendicular magnetic field component, it was also considered the inclusion of a parallel component for the magnetic field, which produces an enhancement of the Zeeman energy term and an effective spin polarization of the system. We see here that, even in the absence of a parallel component of the magnetic field, we can also find a similar structure. It is quite surprising that no such structure has been reported before in the earlier literature of the GN model in a magnetic field. Finally, it is interesting to note that within the OPT the range of μ values for which the global minimum happens at $\bar{\sigma}_2$ is about one-third of the interval predicted by the LN approximation.

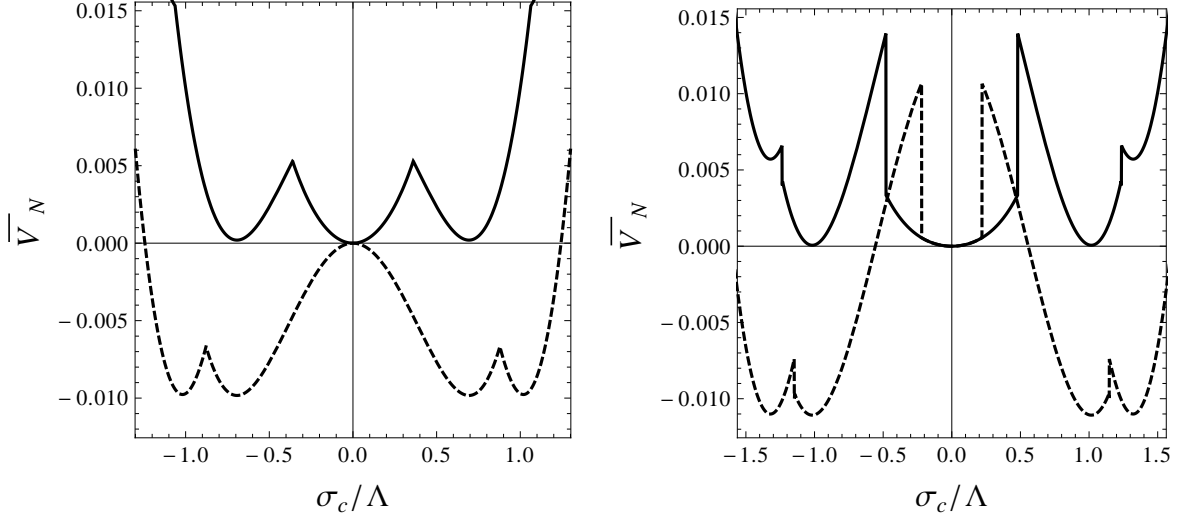


FIG. 6: The (normalized) effective potential (for $\lambda < 0$) at $T = 0$ and $eB = 0.5\Lambda^2$ for the LN case (the plot on the left) and for the OPT (the plot on the right) with $N = 2$. The dashed line is for $\mu \simeq 0.878\Lambda$ in LN case, while in the OPT it is $\mu \simeq 1.02\Lambda$. The solid line is for $\mu \simeq 1.063\Lambda$ in LN case, while in the OPT it is $\mu \simeq 1.09\Lambda$.

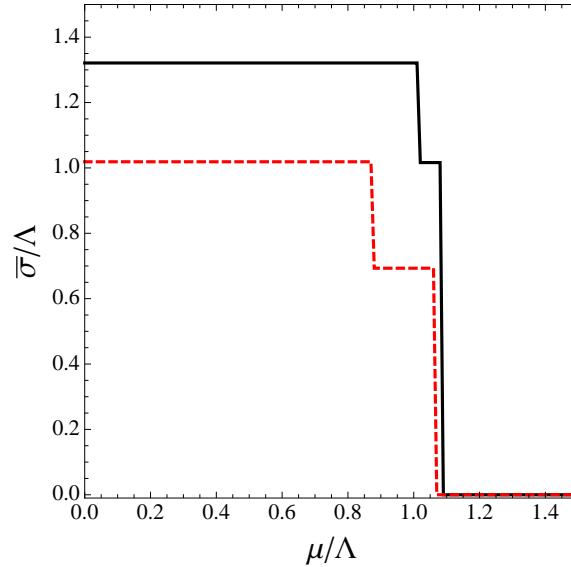


FIG. 7: The order parameter $\bar{\sigma}/\Lambda$ as a function of μ/Λ for $eB = 0.5\Lambda^2$ at $T = 0$. The figure illustrates the discontinuities observed in Fig. 7 for the case $\lambda < 0$. Within the OPT the range of μ values for which the intermediate global minimum happens is about one-third of the interval predicted by the LN approximation.

In order to better understand these transitions we offer Fig. 8, which shows the many discontinuities associated with the de Haas–van Alphen oscillations, which are produced when more Landau levels are filled as μ increases. The

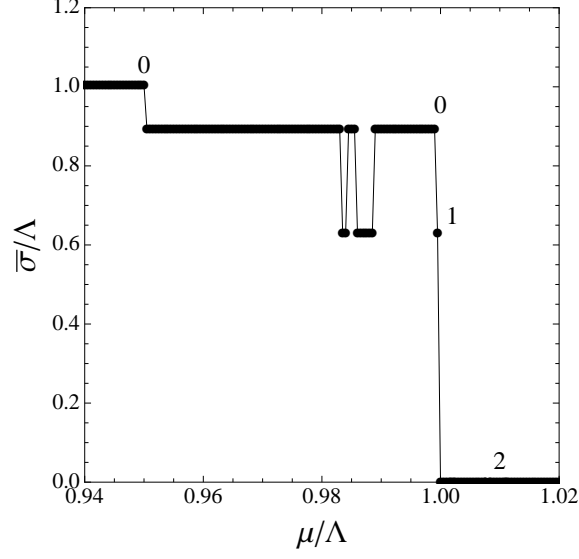


FIG. 8: The order parameter $\bar{\sigma}/\Lambda$ as a function of μ/Λ for $eB = 0.2\Lambda^2$ at $T = 0$ at large N for $\lambda < 0$. The figure illustrates the many discontinuities associated with the de Haas–van Alphen oscillations. The numbers indicate which is the highest filled Landau level for each $\bar{\sigma}$. After the transition to $\bar{\sigma} = 0$, the levels higher than $j = 2$ can be filled by increasing μ .

numbers represent the highest Landau level which for large N , at $T = 0$, is given by

$$J_{max} = \frac{\mu^2 - \bar{\sigma}^2}{2eB} , \quad (4.25)$$

or the nearest integer. The first transition occurs from $J_{max} = 0$ to $J_{max} = 0$ and is produced when $\mu > \bar{\sigma}$, turning on all the Heaviside step functions that appear in the free energy at $T = 0$. The subsequent transitions occur when a different J_{max} is reached. For $eB \geq 0$ the only transition is from $J_{max} = 0$ to $J_{max} = 0$, since this magnetic field (which happened to be of the order of the gap value) is high enough so that only the LLL is always occupied. For $\Lambda^2 > eB \gtrsim 0.4\Lambda^2$ there is a transition from $J_{max} = 0$ to $J_{max} = 0$ associated with $\theta(\mu - \bar{\sigma}) = 1$ and then a second associated with $J_{max} = 0 \rightarrow 1$. Exactly this type of behavior is observed in Fig. 7 for the case of $eB = 0.5\Lambda^2$, which can now be better understood. Then, for $0.4\Lambda^2 > eB \geq 0.2\Lambda^2$ we observe the type of behavior shown in Fig. 8 with the transition that restores chiral symmetry happening at $J_{max} = 2$. For $0 < eB \leq 0.2\Lambda^2$ there are even more transitions since more levels can be filled. For example, at $eB = 0.1\Lambda^2$ chiral symmetry is completely restored ($\bar{\sigma} = 0$) when $J_{max} = 5$. Thus, in summary, for all eB values a first transition occurs due to a nonvanishing value of $\theta(\mu - \bar{\sigma})$. If $eB \geq \Lambda^2$ this is the only transition and only the LLL is always filled, producing a smooth behavior for $\bar{\sigma}$ and μ_c . In the range $0 < eB < \Lambda^2$ there is also a first discontinuity in the value of $\bar{\sigma}$ due to a nonvanishing value of $\theta(\mu - \bar{\sigma})$, but then, since eB is small, there can be subsequent discontinuities in $\bar{\sigma}$ due to the jumps among the integer values of J_{max} , which accounts for the oscillations and discontinuities we have observed at $\lambda < 0$ for small eB . When $\lambda > 0$ and eB , the small chiral symmetry is restored only due to $\theta(\mu - \bar{\sigma}) = 1$ and the filling of higher Landau levels only occurs after $\bar{\sigma} = 0$ by increasing μ . Appendix B shows how these oscillations can be further understood by means of Poisson's summation formula.

D. $T \neq 0$ and $\mu \neq 0$ case

Finally, in the case of finite temperature and chemical potential, we have the effective potential as given by Eq. (3.6). In this case, we search for points in the phase diagram in the plane (T, μ) , corresponding to either a first-order or a second-order phase transition. Recall that in a first-order transition the effective potential develops different minima, $\bar{\sigma}^{(1)} \neq \bar{\sigma}^{(2)}$, where one of them is a local minimum associated with metastability, while the other is a global minimum. These minima can get degenerate for some values of the parameters. For a given value of the magnetic field the first-order transition points in the (T, μ) plane can be determined from the condition of degeneracy of the minima of the effective potential,

$$V_{\text{eff}}(\bar{\sigma}^{(1)}, B, T_c, \mu_c) = V_{\text{eff}}(\bar{\sigma}^{(2)}, B, T_c, \mu_c) . \quad (4.26)$$

One of the minima is, in general, the trivial solution, $\bar{\sigma} = 0$, which then facilitates the determination of the first-order transition points. However, as noticed in the previous subsection, at low magnetic fields $eB \lesssim \Lambda^2$, other minima can emerge and, thus, at low magnetic fields the determination of the transition points must be done with care.

In a first-order phase transition we then have that the minima $\bar{\sigma}$ change discontinuously at the transition point. On the other hand, the second-order phase transition critical points are found when the nontrivial minimum $\bar{\sigma}$ changes continuously and vanishes at the transition point. The point where the second-order transition line meets the first-order one, defines a tricritical point. The second-order and tricritical points are mostly easily found by using a Landau expansion for the effective potential, which is valid for small values of the order parameter. This is the case close to a second-order or tricritical point. The Landau's expansion (for small σ_c) for V_{eff} can be expressed in the general form

$$V_{\text{eff}}(\sigma_c, B, \mu, T) \simeq V_0 + \frac{1}{2}a(B, \mu, T) \sigma_c^2 + \frac{1}{4}b(B, \mu, T) \sigma_c^4 + \frac{1}{6}c(B, \mu, T) \sigma_c^6 , \quad (4.27)$$

where V_0 is a constant (independent of the order parameter) energy term. Note that only even powers of σ_c are allowed due to the original chiral symmetry of the model. The coefficients a, b , and c appearing in Eq. (4.27) can be obtained, respectively, by a second, fourth, and sixth derivative of the effective potential expansion around $\sigma_c = 0$. Higher-order terms in the expansion (4.27) can be verified to be much smaller than the first-order terms and can then be consistently neglected. In particular, note that a tricritical point can emerge whenever we have three phases coexisting simultaneously.

From Eq. (4.27), a second-order phase transition follows when the coefficient of the quadratic term vanishes ($a = 0$) and $b > 0, c > 0$. A first-order transition happens for the case of $b < 0, c > 0$. The tricritical point is found when both the quadratic and quartic coefficients in Eq. (4.27) vanish, $a = b = 0$ (with $c > 0$). Thus, Eq. (4.27) offers a simple and immediate way for analyzing the phase structure of our model. For instance, to obtain T_c at $\mu = 0$ one only needs to consider Eq. (4.27) to order σ_c^4 with $b > 0$ to assure that the potential is bounded from below. Then, the solution of $a(B, 0, T_c) = 0$ sets the critical temperature. However, in order to use Landau's expansion we must have V_{eff} in terms of σ_c, μ and T only (apart from N and the scale Λ , of course). In principle, this can be done by using the PMS relation, Eq. (4.1). Even though at finite N , $\bar{\eta}$ depends on σ_c in a highly nonlinear way, Eq. (4.1) can be easily solved numerically by iteration in a very efficient way (see, e.g., Ref. [26]). For example, at the first iteration, the use of the approximate PMS solution obtained by using the large- N solution $\eta = \sigma_c$ within higher-order $\mathcal{O}(\lambda/N)$ terms,

$$\bar{\eta} \simeq \sigma_c + \frac{\lambda}{2N} \left[\frac{\partial I_1}{\partial \eta} + \frac{\left(\frac{\partial I_1}{\partial \mu} \right) \left(\frac{\partial^2 I_1}{\partial \eta \partial \mu} \right)}{\frac{\partial^2 I_1}{\partial \eta^2}} \right] \Big|_{\eta=\sigma_c} , \quad (4.28)$$

is already able to produce results for the tricritical points within a less than 1% difference with respect to a full numerical calculation. Furthermore, if the second term inside the square brackets in Eq. (4.28) involving the variation of the I_1 term with respect to the chemical potential is much smaller than the first term, it can be neglected and this can make the PMS calculation procedure much simpler. In all cases we have checked the applicability of the use of this simplified form compared with the complete expression (4.28) and used it whenever possible to simplify the numerical calculations. Following this procedure, we obtain the tricritical point as a function of the magnetic field.

In Fig. 9 we give the results for the chemical potential as a function of the magnetic field at the tricritical point, for the cases of negative and positive couplings, for both the LN and OPT (at $N = 2$) cases. Interestingly enough, the LN results for $\lambda < 0$ (right panel) display exactly the same qualitative behavior found in Ref. [40], where the MFA was applied to the three-flavor NJL model in 3+1 dimensions. Note again from this figure the effect of the IMC, similar to the one seen in Fig. 4. The figure shows that μ_{tric} in the OPT case only decreases with B . Again, as in the $T = 0$ case discussed in Sec. IV C, this result could be a sign of the importance brought in by the OPT $\lambda \langle \psi^\dagger \psi \rangle^2 / N$ type of corrections, which start to play an important role in this region of intermediate to large charge asymmetries. For $\lambda > 0$ the right panel of Fig. 9 shows that both the OPT and the LN approximation predict that μ_{tric} always increase with B and that the OPT predicted values are always higher than the LN ones.

In Fig. 10 we give the results for the temperature at the tricritical point as a function of the magnetic field, for the cases of negative (right panel) and positive couplings (left panel), for both the LN and OPT (at $N = 2$) cases. Let us start by discussing the case of negative coupling at vanishing magnetic field, where the figure shows that the LN predicts $T_{\text{tric}} = 0$, while the OPT predicts $T_{\text{tric}} \simeq 0.28 \Lambda$. As we have already discussed (see also Refs. [23, 26])

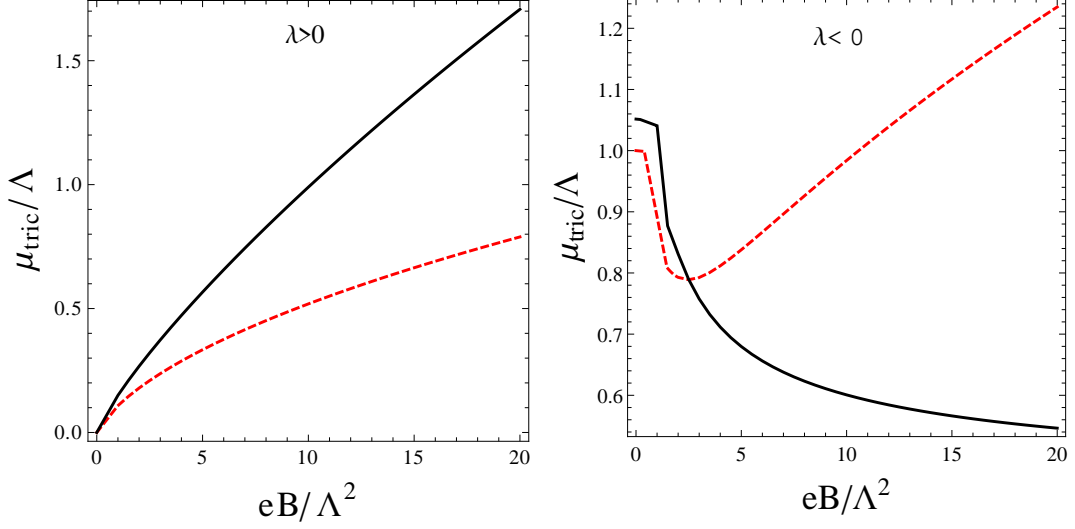


FIG. 9: The chemical potential at the tricritical point for $\lambda > 0$ (the plot on the left) and for $\lambda < 0$ (the plot on the right), for the LN (dashed line) and for the OPT (solid line) with $N = 2$.

this LN result for $B = 0$ can be shown to be wrong due to universality arguments, while the OPT predicted values for finite N are within the range estimated (but not pinpointed) by Monte-Carlo simulations [24]. Despite these important quantitative differences, both approximations show that T_{tric} increases with the magnetic field.

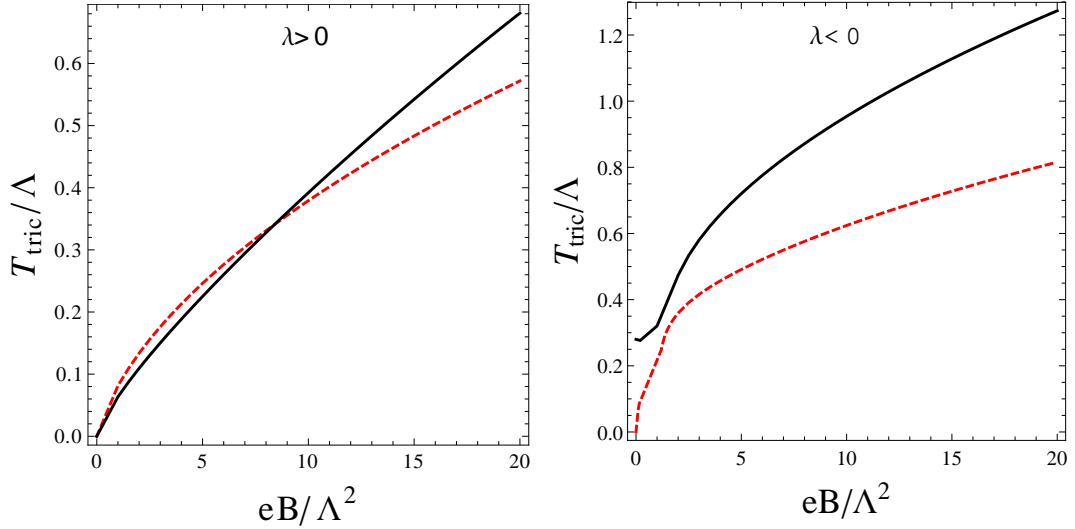


FIG. 10: The temperature at the tricritical point for $\lambda > 0$ (the plot on the left) and for $\lambda < 0$ (the plot on the right), for the LN (dashed line) and for the OPT (solid line) with $N = 2$.

Next, in Fig. 11, we show the complete phase diagram for the LN and OPT cases for representative values of the magnetic field. Note that in the LN case for $B = 0$ and negative coupling, there is only a second-order transition line in the (μ, T) phase diagram, with the exception of the pair $T = 0$ and $\mu = \Lambda$, which correspond to a first-order transition point. As shown in Ref. [23], it is only by including beyond mean-field effects that a first-order transition line (along with the tricritical point) emerges, in agreement with the expectations based on the results for the GN model in 1+1 dimensions and also for the NJL model in 3+1 dimensions. Note, however, that for nonvanishing magnetic fields, a tricritical point is produced even in the LN case. For positive couplings, recall that a chiral phase transition is only possible for nonvanishing magnetic fields [12].

Figure 11 shows that for both a negative or a positive coupling the presence of a magnetic field always increases the

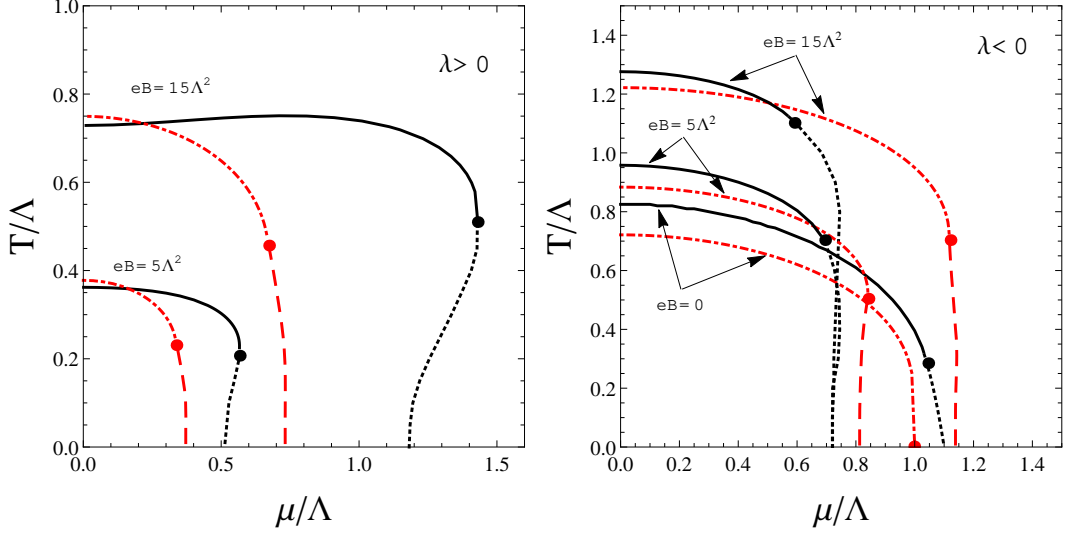


FIG. 11: The phase diagram for $\lambda > 0$ (the plot on the left) and for $\lambda < 0$ (the plot on the right). All cases are for $N = 2$. The solid lines indicate second-order phase transition lines in the OPT case, while dashed-dotted lines in the LN case. The first-order lines are indicated by dotted lines in the OPT case and by long dashed lines in the LN case. Where the second-order line meets the first-order line (the tricritical point) is indicated by the large dot.

size of the first-order transitions. In the OPT case this increase is even more pronounced since the term $\lambda\langle\psi^+\psi\rangle^2/N$ enhances this type of transitions when $\lambda < 0$ and the $1/N$ correction acts as an attractive vector term [45]. In both the OPT and LN cases and for any sign for the coupling, the CSB region tends to get larger as B grows.

Note that there is magnetic catalysis in T_c and inverse catalysis in μ_c for $\lambda < 0$, but only catalysis for $\lambda > 0$ in the OPT case. For the LN case and $\lambda < 0$, the inverse magnetic catalysis only happens until some value of B and then there is only catalysis beyond that value of magnetic field. So for $eB \gtrsim 5\Lambda^2$ or so, the CSB region in the LN case will become always larger than in the OPT when $\lambda < 0$, while it is the opposite when $\lambda > 0$, where $\lambda\langle\psi^+\psi\rangle^2/N$ acts as a repulsive vector term, which competes with the effect of the magnetic field by enhancing more the CSB region in the OPT case than in the LN case.

V. CONCLUSIONS

In this work we have analyzed the effects of a nonvanishing constant magnetic field (applied perpendicularly to the plane of the system) on the phase structure of the massless discrete (2+1)-dimensional GN model, including contributions which go beyond the LN (or mean field) approximation. Here we have used the OPT method, which has already been successfully used before to study the properties of this model in the absence of a magnetic field. Both the cases of positive and negative four-fermion coupling have been studied.

We have produced some novel results concerning the phase structure of the model in the presence of a magnetic field. For negative couplings, we have shown that at low magnetic fields ($eB \lesssim \Lambda^2$) a rich structure of phases can emerge. In this case, it is possible to have intermediate transitions to nonvanishing values of the chiral vacuum expectation value. These transitions happen in the LN case, something that has not been previously noted in the literature⁷ and remains also when including corrections beyond the LN approximation, as we have shown by using the OPT method. Therefore, these intermediate transitions are not an artifact of the LN approximation. We have also traced the origin of these intermediate transitions as being a consequence of the magnetic de Haas–van Alphen oscillations that arise at low values of the magnetic field, $eB \lesssim \Lambda^2$ and for negative values of the coupling constant.

⁷ Recently, in Ref. [44] a similar structure of phase transitions has also been found, though in that reference it was also included a parallel component for the magnetic field, which is then able to further enhance these intermediate phases and also to produce reentrant phase transitions. However, in the absence of the perpendicular component of the magnetic field, the intermediate and reentrant phases are both absent [46].

As for the effect of the magnetic field on the phase structure of the model, we have shown two distinct effects depending on the sign of the coupling constant. For either positive or negative couplings, we still have an enhancement of the chiral-broken-symmetry region, as expected in general from the magnetic catalysis effect. However, when the coupling is negative, beyond some value of the magnetic field the chiral broken region is always smaller in the OPT case than in the LN, while for positive coupling the reverse is observed, with the OPT always producing a larger broken symmetry region. The tricritical points tend to be also enhanced in general by the presence of the magnetic field, with the results obtained in the OPT larger than in the LN case. The exception is the value of the chemical potential at the tricritical point, μ_{tricrit} when the coupling is negative. When $\lambda < 0$, in the LN case μ_{tricrit} tends to be strongly suppressed by the magnetic field initially, until for $eB \gtrsim 2\Lambda^2$ it turns again to be enhanced by the magnetic field. This decrease of the critical chemical potential with the magnetic field, the inverse magnetic catalysis effect, has some similarity with the phenomenon seen in the NJL model and discussed in details recently in Ref. [30]. But in our case it originates from the OPT $\lambda\langle\psi^\dagger\psi\rangle/N$ corrections beyond LN, as explained in Sec. IV C. In the OPT case μ_{tricrit} continues to decrease for very large magnetic fields. Thus, the inverse magnetic catalysis remains unsuppressed even for large values of the magnetic field in the OPT context, which is opposite to what is seen in the LN case. Note also that inverse magnetic catalysis is seen to operate only on the critical chemical potential values, while the critical temperature still shows only the standard magnetic catalysis, always increasing with B . This same trend also applies to the coexistence chemical potential when $T = 0$, where, for $\lambda < 0$, the OPT shows an inverse magnetic catalysis effect even for large magnetic fields, while in the LN case, the chemical potential only decreases for relatively small values of the magnetic field and grows for $eB \gtrsim 2\Lambda^2$. At $\mu = 0$, the critical temperature is seen only to increase with the magnetic field in both the OPT and LN cases, independently of the sign of the coupling constant. The stability of the order- δ results for the same model, at $B = 0$, has been addressed in Ref. [23] and the outcome of that investigation allows us to believe that our present results, at $B \neq 0$, should also be stable against the inclusion higher-order corrections.

It is tempting to compare our results with recent lattice results for the QCD chiral crossover temperature as function of B . The first lattice studies [47] considered two quark flavors, with high values of pion masses ($m_\pi = 200 - 400$ MeV), and have shown that the critical temperature should increase with B . However, an improved lattice simulation [48], which considered 2+1 quark flavors at physical pion mass values ($m_\pi = 140$ MeV), together with an extrapolation to the continuum, predicted that the critical temperature should decrease with B . Since then, most models have tried to reproduce these lattice results, showing, however, that the critical temperature only increases with the magnetic field. Since most model results were obtained within the LN/MFA, one may wonder if the discrepancy could not be resolved by going beyond this approximation. Our results indicate that this may not be sufficient and that other effects besides going beyond the LN approximation are required.

We hope that our findings will give further insights in applications that employ four-fermion models in the description of planar condensed matter systems, which we intend to further explore in the future.

Appendix A: Summing Matsubara frequencies, Landau levels and related formulas

Let us derive here the momentum integrals appearing in the expression for the effective potential (3.4) and then give the I_i , $i = 1, 2, 3$, integrals Eqs. (3.7), (3.8) and (3.9). Using the replacements (3.5), $p_0 \rightarrow i(\omega_\nu - i\mu)$ and $\mathbf{p}^2 \rightarrow 2jeB$, with $\omega_\nu = (2\nu + 1)\pi T$, $\nu = 0, \pm 1, \pm 2, \dots$, are the Matsubara frequencies for fermions and j labels the LLs. The integral I_1 is defined as

$$\begin{aligned} I_1 &= i \int_p \ln(P^2 - \eta^2) \\ &= -T \sum_{\nu=-\infty}^{+\infty} \frac{eB}{4\pi} \sum_{j=0}^{\infty} \alpha_j \ln[(\omega_\nu - i\mu)^2 + E_j^2] \end{aligned} \quad (\text{A1})$$

where $E_j = \sqrt{2jeB + \eta^2}$ and $\alpha_j = 2 - \delta_{j,0}$. Performing the Matsubara sum one gets

$$I_1 = -\frac{eB}{4\pi} \sum_{j=0}^{\infty} \alpha_j \left\{ E_j + T \ln[1 + e^{-(E_j + \mu)/T}] + T \ln[1 + e^{-(E_j - \mu)/T}] \right\}. \quad (\text{A2})$$

In the same way, we have that

$$\begin{aligned}
I_2 &= i \int_p \frac{1}{P^2 - \eta^2} \\
&= \frac{eB}{8\pi} \sum_{j=0}^{\infty} \alpha_j \left\{ \frac{1}{E_j} - \frac{1}{E_j[1 + e^{(E_j + \mu)/T}]} - \frac{1}{E_j[1 + e^{(E_j - \mu)/T}]} \right\}, \tag{A3}
\end{aligned}$$

while the last momentum integral remaining that we need is

$$\begin{aligned}
I_3 &= -i \int_p \frac{P_0}{P^2 - \eta^2} \\
&= \frac{eB}{8\pi} \sum_{j=0}^{\infty} \alpha_j \left[\frac{\sinh(\mu/T)}{\cosh(\mu/T) + \cosh(E_j/T)} \right] \\
&= \frac{eB}{8\pi} \sum_{j=0}^{\infty} \alpha_j \left[\frac{1}{e^{(E_j - \mu)/T} + 1} - \frac{1}{e^{(E_j + \mu)/T} + 1} \right]. \tag{A4}
\end{aligned}$$

There is a very convenient trick to perform the sum over Landau levels for the T, μ independent terms which can be expressed in a closed form by means of Riemann–Hurwitz zeta functions [37]. For example, consider the T, μ independent term on the right-hand side of Eq. (A2). By adding and subtracting a lowest Landau energy level term, E_0 , to it one can write

$$-\frac{eB}{4\pi} \sum_{j=0}^{\infty} \alpha_j E_j + \frac{eB}{4\pi} E_0 - \frac{eB}{4\pi} E_0 = \frac{eB|\eta|}{4\pi} - \frac{(2eB)^{3/2}}{4\pi} \sum_{j=0}^{\infty} \left[j + \frac{\eta^2}{2eB} \right]^{1/2}. \tag{A5}$$

The infinite sum can be related to the Riemann–Hurwitz zeta function Eq. (3.10), yielding

$$-\frac{eB}{4\pi} \sum_{j=0}^{\infty} \alpha_j E_j = \frac{eB|\eta|}{4\pi} - \frac{(2eB)^{3/2}}{4\pi} \zeta \left(-\frac{1}{2}, \frac{\eta^2}{2eB} \right). \tag{A6}$$

The same technique, when applied to the T and μ independent term of Eq. (A3), gives

$$\frac{eB}{8\pi} \sum_{j=0}^{\infty} \alpha_j \frac{1}{E_j} = -\frac{eB}{8\pi|\eta|} + (2eB)^{1/2} \frac{1}{8\pi} \zeta \left(\frac{1}{2}, \frac{\eta^2}{2eB} \right). \tag{A7}$$

The same types of manipulations can be applied to divergent terms, as discussed in Refs. [40, 41].

It is also useful to have the limiting cases for the functions I_i when $T = 0$ and/or $\mu = 0$. Taking the $T = 0$ limit in Eqs. (A2), (A3) and (A4), we obtain

$$I_1(\eta, B, T, \mu) \xrightarrow{T \rightarrow 0} \frac{eB}{4\pi} |\eta| - \frac{(2eB)^{3/2}}{4\pi} \zeta \left(-\frac{1}{2}, \frac{\eta^2}{2eB} \right) - \frac{eB}{4\pi} \sum_{j=0}^{J_{\max}} \alpha_j (\mu - E_j) \theta(\mu - |\eta|), \tag{A8}$$

$$I_2(\eta, B, T, \mu) \xrightarrow{T \rightarrow 0} -\frac{eB}{8\pi|\eta|} + \frac{(2eB)^{1/2}}{8\pi} \zeta \left(\frac{1}{2}, \frac{\eta^2}{2eB} \right) - \frac{eB}{8\pi} \sum_{j=0}^{J_{\max}} \alpha_j \frac{1}{E_j} \theta(\mu - |\eta|), \tag{A9}$$

$$I_3(\eta, B, T, \mu) \xrightarrow{T \rightarrow 0} \frac{eB}{8\pi} \theta(\mu - |\eta|) + \frac{eB}{4\pi} \text{Int} \left(\left\lfloor \frac{\mu^2 - \eta^2}{2eB} \right\rfloor \right) \theta(\mu - |\eta|), \tag{A10}$$

where in the above equations $J_{\max} = \text{Int}((\mu^2 - \eta^2)/(2eB))$ and $\text{Int}(x)$ means the integer part of x .

Taking the $\mu = 0$ limit in Eqs. (A2), (A3) and (A4), we obtain

$$I_1(\eta, B, T, \mu) \xrightarrow{\mu \rightarrow 0} \frac{eB|\eta|}{4\pi} - \frac{(2eB)^{3/2}}{4\pi} \zeta\left(-\frac{1}{2}, \frac{\eta^2}{2eB}\right) - \frac{eBT}{2\pi} \sum_{j=0}^{\infty} \alpha_j \ln\left(1 + e^{-E_j/T}\right), \quad (\text{A11})$$

$$I_2(\eta, B, T, \mu) \xrightarrow{\mu \rightarrow 0} -\frac{eB}{8\pi|\eta|} + \frac{(2eB)^{1/2}}{8\pi} \zeta\left(\frac{1}{2}, \frac{\eta^2}{2eB}\right) - \frac{eB}{4\pi} \sum_{j=0}^{\infty} \alpha_j \frac{1}{E_j (1 + e^{E_j/T})}, \quad (\text{A12})$$

$$I_3(\eta, B, T, \mu) \xrightarrow{\mu \rightarrow 0} 0, \quad (\text{A13})$$

while for $T = 0$ and $\mu = 0$, we obtain

$$I_1(\eta, B, T, \mu) \xrightarrow{T, \mu \rightarrow 0} \frac{eB|\eta|}{4\pi} - \frac{(2eB)^{3/2}}{4\pi} \zeta\left(-\frac{1}{2}, \frac{\eta^2}{2eB}\right), \quad (\text{A14})$$

$$I_2(\eta, B, T, \mu) \xrightarrow{T, \mu \rightarrow 0} -\frac{eB}{8\pi|\eta|} + \frac{(2eB)^{1/2}}{8\pi} \zeta\left(\frac{1}{2}, \frac{\eta^2}{2eB}\right), \quad (\text{A15})$$

$$I_3(\eta, B, T, \mu) \xrightarrow{T, \mu \rightarrow 0} 0. \quad (\text{A16})$$

Appendix B: Low- B behavior and de Haas–van Alphen oscillations

It is instructive to analyze the origin of the oscillating behavior at low B found in the case of $T = 0$ and $\lambda < 0$ in Sec. IV C. Since the terms I_2 and I_3 are directly derived from I_1 , it is enough for our purposes here to analyze the low- B behavior of only I_1 . The $\mu \neq 0$ dependent part of I_1 at $T = 0$, from Eq. (A8), is given by

$$\begin{aligned} I_1^{\mu \neq 0, T=0} &= -\frac{eB}{4\pi} \sum_{j=0}^{J_{\max}} \alpha_j (\mu - E_j) \theta(\mu - |\eta|) \\ &= -\frac{eB}{4\pi} \sum_{j=0}^{\infty} \alpha_j (\mu - E_j) \theta(\mu - E_j) \\ &= -\frac{eB}{4\pi} \sum_{j=-\infty}^{\infty} (\mu - E_{|j|}) \theta(\mu - E_{|j|}) \\ &= -\frac{eB}{2\pi} \sum_{n=-\infty}^{\infty} \int_0^{J_{\max}} dy [\mu - E(y)] \cos(2\pi ny) \theta(\mu - |\eta|), \end{aligned} \quad (\text{B1})$$

where $E(y) = \sqrt{2eBy + \eta^2}$ and in the last line in the above equation we have made use of the Poisson's summation formula [49],

$$\sum_{j=-\infty}^{\infty} f(j) = \sum_{n=-\infty}^{\infty} \int_{-\infty}^{\infty} dy f(y) e^{-2\pi i ny}. \quad (\text{B2})$$

Performing the integral in Eq. (B1), we find

$$\begin{aligned} I_1^{\mu \neq 0, T=0} &= -\frac{1}{4\pi} \left[\frac{\mu^3}{3} - \mu\eta^2 + \frac{2}{3}|\eta|^3 + \frac{eB}{\pi}|\eta| \sum_{n=1}^{\infty} \frac{1}{n} P_2\left(\frac{n\pi}{eB}\eta^2\right) \right] \theta(\mu - |\eta|) \\ &+ \frac{eB}{4\pi^2} \mu \sum_{n=1}^{\infty} \frac{1}{n} \left\{ P_2\left(\frac{n\pi}{eB}\mu^2\right) \cos\left[\frac{n\pi}{eB}(\eta^2 - \mu^2)\right] \right. \\ &+ \left. Q_2\left(\frac{n\pi}{eB}\mu^2\right) \sin\left[\frac{n\pi}{eB}(\eta^2 - \mu^2)\right] \right\} \theta(\mu - |\eta|), \end{aligned} \quad (\text{B3})$$

where the functions $P_2(x)$ and $Q_2(x)$ are defined as

$$\begin{aligned} Q_2(x) &= \sqrt{\frac{2\pi}{x}} \left\{ \left[C_2(x) - \frac{1}{2} \right] \cos(x) + \left[S_2(x) - \frac{1}{2} \right] \sin(x) \right\}, \\ P_2(x) &= \sqrt{\frac{2\pi}{x}} \left\{ \left[C_2(x) - \frac{1}{2} \right] \sin(x) - \left[S_2(x) - \frac{1}{2} \right] \cos(x) \right\}, \end{aligned} \quad (\text{B4})$$

and $C_2(x)$ and $S_2(x)$ are the Fresnel integrals [50],

$$\begin{aligned} C_2(x) &\equiv \frac{1}{\sqrt{2\pi}} \int_0^x dt \, t^{-\frac{1}{2}} \cos t, \\ S_2(x) &\equiv \frac{1}{\sqrt{2\pi}} \int_0^x dt \, t^{-\frac{1}{2}} \sin t. \end{aligned} \quad (\text{B5})$$

In Eq. (B3) the oscillatory character of the effective potential at low- B becomes explicit, as the origin of the de Haas–van Alphen oscillations in magnetized systems. For $\lambda < 0$ in the symmetry broken phase, as far $\mu > \eta$ and since η is determined from the PMS solution (4.16), $\bar{\eta} \approx \bar{\sigma} \approx \Lambda$, we have that for $eB \lesssim \Lambda^2$ all quantities depending on I_1 will exhibit an oscillatory behavior, with the different basic functions in Eq. (B3) of periods $\propto (eB)^{-1}$ characteristic of de Haas–van Alphen oscillations. This determines the low- B behavior seen in Figs. 4 and 5, as well the multiple minima structure exhibited by the effective potential for values of magnetic field $eB \lesssim \Lambda^2$ and shown in the example given by Fig. 6. When $\lambda > 0$, we know that in the absence of a magnetic field there is no chiral symmetry breaking. However, when $B \neq 0$, magnetic catalysis induces chiral symmetry breaking and, as first shown in Ref. [12], in the LN case, the vacuum expectation value for σ is $\bar{\sigma} \sim eB/\Lambda$, but we have that $\bar{\eta} \sim \bar{\sigma}$ and then, for $\mu > \eta \sim \bar{\sigma}$, the magnetic oscillations become highly suppressed when $\lambda > 0$. This is why we do not see (or hardly can see any) oscillations in this case.

Acknowledgments

M.B.P. and R.O.R. are partially supported by Conselho Nacional de Desenvolvimento Científico e Tecnológico (CNPq). R.O.R. is also partially supported by a research grant from Fundação Carlos Chagas Filho de Amparo à Pesquisa do Estado do Rio de Janeiro (FAPERJ) and M.B.P. is also partially supported by Fundação de Amparo à Pesquisa e Inovação do Estado de Santa Catarina (FAPESC).

-
- [1] B. Rosenstein, B. Warr and S. H. Park, Phys. Rep. **205**, 59 (1991).
 - [2] Y. Nambu and G. Jona-Lasinio, Phys. Rev. **122**, 345 (1961) ; Phys. Rev. **124**, 246 (1961).
 - [3] D. J. Gross and A. Neveu, Phys. Rev. D **10**, 3235 (1974).
 - [4] U. Wolff, Phys. Lett. B **157**, 303 (1985); K. G. Klimenko, Z. Phys. **C37**, 457 (1988); B. Rosenstein, B. J. Warr and S. H. Park, Phys. Rev. D **39**, 3088 (1989); A. Barducci, R. Casalbuoni, M. Modugno, G. Pettini and R. Gatto, Phys. Rev. D **51**, 3042 (1995); F. C. Khanna, A. P. C. Malbouisson, J. M. C. Malbouisson and A. E. Santana, Europhys. Lett. **92**, 1101 (2010).
 - [5] D. V. Khveshchenko, Phys. Rev. Lett. **87**, 206401 (2001); E. V. Gorbar, V. P. Gusynin, V. A. Miransky and I. A. Shovkovy, Phys. Rev. B **66**, 045108 (2002); H. Leal and D. V. Khveshchenko, Nucl. Phys. B **687**, 323 (2004).
 - [6] V. P. Gusynin and S. G. Sharapov, Phys. Rev. Lett. **95**, 146801 (2005); V. P. Gusynin, V. A. Miransky, S. G. Sharapov and I. A. Shovkovy, Phys. Rev. B **74**, 195429 (2006).
 - [7] G. W. Semenoff, I. A. Shovkovy and L. C. R. Wijewardhana, Mod. Phys. Lett. A **13**, 1143 (1998); K. Krishana, N. P. Ong, Y. Zhang, et al. 1999, Phys. Rev. Lett. **82**, 5108 (1999); D. V. Khveshchenko, W. F. Shively, Phys. Rev. B **73**, 115104 (2006).
 - [8] R. Duncan and C. Thompson, Astrophys. J. Lett., **392**, L9 (1992); C. Kouveliotou et al., Nature **393**, 235 (1998).
 - [9] K. Fukushima, D. E. Kharzeev and H. J. Warringa, Phys. Rev. D **78**, 074033 (2008); D. E. Kharzeev, L.D. McLerran and H. J. Warringa, Nucl. Phys. A **803**, 227 (2008); D. E. Kharzeev and H. J. Warringa, Phys. Rev. D **80**, 0304028 (2009); D. E. Kharzeev, Nucl. Phys. A **830**, 543c (2009).
 - [10] T. Vaschupati, Phys. Lett. B **265**, 258 (1991).
 - [11] K. Fukushima, J. Phys. G **39**, 013101 (2012); K. Tuchin, Adv. High Energy Phys. **2013**, 490495 (2013).

- [12] K. G. Klimenko, Theor. Math. Phys. **90**, 1 (1992) [Teor. Mat. Fiz. **90**, 3 (1992)]; Z. Phys. C **54**, 323 (1992); Theor. Math. Phys. **89**, 1161 (1992) [Teor. Mat. Fiz. **89**, 211 (1991)].
- [13] V. P. Gusynin, V. A. Miransky and I. A. Shovkovy, Phys. Rev. Lett. **73**, 3499 (1994) [Erratum-ibid. **76**, 1005 (1996)]; Phys. Rev. D **52**, 4718 (1995).
- [14] D. C. Duarte, R. L. S. Farias and R. O. Ramos, Phys. Rev. D **84**, 083525 (2011); A. Ayala, M. Loewe, J. C. Rojas and C. Villavicencio, Phys. Rev. D **86**, 076006 (2012).
- [15] A. Okopinska, Phys. Rev. D **35**, 1835 (1987); M. Moshe and A. Duncan, Phys. Lett. **B215**, 352 (1988); S. Chiku and T. Hatsuda, Phys. Rev. D **58**, 076001 (1998).
- [16] R. Seznec and J. Zinn-Justin, J. Math. Phys. **20**, 1398 (1979); J. C. Le Guillou and J. Zinn-Justin, Ann. Phys. **147**, 57 (1983); V. I. Yukalov, Teor. Mat. Fiz. **28**, 92 (1976); W. E. Caswell, Ann. Phys. (N.Y) **123**, 153 (1979); I. G. Halliday and P. Suranyi, Phys. Lett. **B85**, 421 (1979); J. Killinbeck, J. Phys. **A14**, 1005 (1981); R. P. Feynman and H. Kleinert, Phys. Rev. A **34**, 5080 (1986); H. F. Jones and M. Moshe, Phys. Lett. **B234**, 492 (1990); A. Neveu, Nucl. Phys. (Proc. Suppl.) **B18**, 242 (1990); V. Yukalov, J. Math. Phys **32**, 1235 (1991); C. M. Bender et al., Phys. Rev. D **45**, 1248 (1992); K. G. Klimenko, Z. Phys. **C60**, 677 (1993); A.N. Sissakian, I. L. Solovtsov and O. P. Solovtsova, Phys. Lett. **B321**, 381 (1994); H. Kleinert, Phys. Rev. D **57**, 2264 (1998); Phys. Lett. **B434**, 74 (1998); for a review, see H. Kleinert and V. Schulte-Frohlinde, *Critical Properties of ϕ^4 -Theories*, Chap. 19 (World Scientific, Singapore 2001).
- [17] F. F. de Souza Cruz, M. B. Pinto and R. O. Ramos, Phys. Rev. B **64**, 014515 (2001); J. -L. Kneur, M. B. Pinto and R. O. Ramos, Phys. Rev. A **68**, 043615 (2003); Phys. Rev. Lett. **89**, 210403 (2002); H. Kleinert, Mod. Phys. Lett. **B17**, 1011 (2003); B. Kastening, Phys. Rev. A **68**, 061601 (2003); Phys. Rev. A **69** (2004) 043613; J. -L. Kneur, A. Neveu and M. B. Pinto, Phys. Rev. A **69**, 053624 (2004); J. -L. Kneur and M. B. Pinto, Phys. Rev. A **71**, 033613 (2005).
- [18] H. Caldas, J. -L. Kneur, M. B. Pinto and R. O. Ramos, Phys. Rev. B **77**, 205109 (2008).
- [19] J. O. Andersen, L. E. Leganger, M. Strickland and N. Su, JHEP **1108**, 053 (2011); J. O. Andersen, M. Strickland and N. Su, JHEP **1008**, 113 (2010).
- [20] J.-L. Kneur and A. Neveu, Phys. Rev. D **81**, 125012 (2010).
- [21] J.-L. Kneur and A. Neveu, Phys. Rev. D **85**, 014005 (2012).
- [22] J.-L. Kneur and A. Neveu, arXiv:1305.6910.
- [23] J. -L. Kneur, M. B. Pinto, R. O. Ramos and E. Staudt, Phys. Rev. D **76**, 045020 (2007).
- [24] J. B. Kogut and C. G. Strouthos, Phys. Rev. D **63**, 054502 (2001).
- [25] S. Hands, K. Kocic and J. B. Kogut, Ann. Phys. **224**, 29 (1993); Nucl. Phys. **B390**, 355 (1993).
- [26] J. -L. Kneur, M. B. Pinto, R. O. Ramos and E. Staudt, Phys. Lett. B **657**, 136 (2007).
- [27] J. -L. Kneur, M. B. Pinto and R. O. Ramos, Phys. Rev. C **81**, 065205 (2010).
- [28] J. -L. Kneur, M. B. Pinto, R. O. Ramos and E. Staudt, Int. J. Mod. Phys. E **21**, 1250017 (2012).
- [29] D. D. Scherer and H. Gies, Phys. Rev. B **85**, 195417 (2012).
- [30] F. Preis, A. Rebhan and A. Schmitt, Lect. Notes Phys. **871**, 51 (2013); F. Preis, A. Rebhan and A. Schmitt, JHEP **1103**, 033 (2011).
- [31] T. W. Appelquist, M. J. Bowick, D. Karabali and L. C. R. Wijewardhana, Phys. Rev. D **33**, 3704 (1986).
- [32] S. Coleman, *Aspects of Symmetry* (Cambridge University Press, Cambridge, 1985).
- [33] J. -L. Kneur, M. B. Pinto and R. O. Ramos, Phys. Rev. D **74**, 125020 (2006).
- [34] M. B. Pinto and R. O. Ramos, Phys. Rev. D **60**, 105005 (1999); Phys. Rev. D **61**, 125016 (2000); R. L. S. Farias, G. Krein and R. O. Ramos, Phys. Rev. D **78**, 065046 (2008).
- [35] P. M. Stevenson, Phys. Rev. D **23**, 2916 (1981).
- [36] R. G. Root, Phys. Rev. D **11**, 831 (1975).
- [37] E. Elizalde, A. D. Odintsov and A. Romeo, *Zeta Regularization Techniques with Applications* (World Scientific, Singapore, 1994).
- [38] A. S. Vshivtsev, K. G. Klimenko and B. V. Magnitsky, Theor. Math. Phys. **106**, 319 (1996) [Teor. Mat. Fiz. **106**, 390 (1996)].
- [39] A. Chodos, K. Everding and D. A. Owen, Phys. Rev. D **42**, 2881 (1990).
- [40] S. S. Avancini, D. P. Menezes, M. B. Pinto and C. Providencia, Phys. Rev. D **85**, 091901 (2012).
- [41] G. N. Ferrari, A. F. Garcia and M. B. Pinto, Phys. Rev. D **86**, 096005 (2012).
- [42] D. Ebert, K.G. Klimenko, M.A. Vdovichenko and A.S. Vshivtsev, Phys. Rev. D **61**, 025005 (2000).
- [43] T. Inagaki, D. Kimura and T. Murata, Prog. Theor. Phys. **111**, 371 (2004).
- [44] R. O. Ramos and P. H. A. Manso, Phys. Rev. D **87**, 125014 (2013).
- [45] K. Fukushima, Phys. Rev. D **78**, 114019 (2008).
- [46] H. Caldas and R. O. Ramos, Phys. Rev. B **80**, 115428 (2009).
- [47] M. D'Elia, S. Mukherjee and F. Sanfilippo, Phys. Rev. D **82**, 051501 (2010).
- [48] G. S. Bali, F. Bruckmann, G. Endrodi, Z. Fodor, S. D. Katz, S. Krieg, A. Schafer and K. K. Szabo, JHEP **1202**, 044 (2012); G. S. Bali, F. Bruckmann, G. Endrodi, Z. Fodor, S. D. Katz and A. Schafer, Phys. Rev. D **86**, 071502 (2012).
- [49] E. W. Weisstein, *Poisson Sum Formula* from <http://mathworld.wolfram.com/PoissonSumFormula.html> (MathWorld—A Wolfram Web Resource.)
- [50] H. Bateman and A. Erdelyi, *Higher Transcendental Functions* (McGraw-Hill, New York, 1953).